IEEE Access
Multidisciplinary | Rapid Review | Open Access Journal

Received January 5, 2019, accepted January 27, 2019, date of publication January 31, 2019, date of current version February 22, 2019.

Digital Object Identifier 10.1109/ACCESS.2019.2896588

Fuzzy Observer-Based Prescribed Performance Control of Vehicle Roll Behavior via Controllable Damper

ZHENFENG WANG[1], (Member, IEEE), YECHEN QIN[2], (Member, IEEE), CHUAN HU[3], MINGMING DONG[2], AND FEI LI[1]

[1]Automotive Engineering Research Institute, China Automotive Technology and Research Center, Tianjin 300300, China
[2]School of Mechanical Engineering, Beijing Institute of Technology, Beijing 100081, China
[3]Department of Mechanical Engineering, The University of Texas at Austin, Austin, TX 78712, USA

Corresponding author: Yechen Qin (qinyechenbit@gmail.com)

This work was supported by the National Natural Science Foundation of China under Grant 51805028.

ABSTRACT This paper presents a novel observer-based control strategy to improve the vehicle roll behavior performance through magneto-rheological (MR) dampers under steering wheel input and various road excitation conditions. Since the vehicle roll with sudden steering input is an essential part of driving safety and possesses inherent nonlinearities, the full-car nonlinear Takagi-Sugeno (T-S) fuzzy model is first established to describe the vehicle roll dynamics considering nonlinear coupling dynamics of tire lateral force and MR damper force under road excitation input. Furthermore, a T-S model-based fuzzy observer is adapted to estimate the vehicle roll angle and roll rate. The stability conditions for the used T-S observer are calculated using linear matrix inequalities (LMIs), and the proposed observer is induced by solving the proposed LMI. Based on the Lyapunov function, sliding mode theory and prescribed performance function, a novel state observer-based prescribed performance control strategy is developed to constrain the controlled vehicle roll angle and roll rate state within the prescribed performance boundaries. Finally, the proposed techniques are validated through the J-turn and Fishhook tests conducted via a high-fidelity CarSim software platform.

INDEX TERMS Vehicle roll dynamics, prescribed performance control, Takagi-Sugeno fuzzy observer, state estimation, vehicle system.

I. INTRODUCTION

Vehicle roll behavior plays a critical role in the safety of vehicle driving. According to the National Highway Traffic Safety Administration (NHTSA), vehicle rollover occurred in about 3% of all passenger-vehicle crashes in 2002, and 33% of all fatalities had vehicle rollover as a contributor in 2014 [1]–[4]. Hence, advanced control algorithms for rollover prevention, such as Roll Stability Control (RSC) systems, are highly desired for vehicle systems [5], [6]. However, since closed-loop realizations are based on the knowledge of many roll angle and roll rate sensors, such systems are commercially unattractive due to the high cost of sensors for measuring these states. Therefore, to save costs, the determination of unmeasurable states for controllable suspension systems is key to the application of such methods [7], [8]. Furthermore, accuracy of state estimation and transient optimal control exert a significant effect on the vehicle roll dynamics control [8]. Based on the above analysis, many approaches have been adopted to improve the vehicle roll dynamic performance [9], [10]. Among them, the Takagi-Sugeno (T-S) control strategy is commonly used to enhance the performance of the controlled system.

The T-S fuzzy model should be introduced first when discussing the T-S observer-based control algorithm. In the 1980s, based on the use of a set of fuzzy rules, the Takagi-Sugeno (T-S) fuzzy model [11] was first presented to describe a global nonlinear system. Since a set of linear models were used in the calculation of nonlinear issues, this approach has been widely applied to the field of vehicle nonlinear system. Dahmani *et al.* [12] used a T-S observer-based robust controller to improve vehicle rollover in critical situations. The nonlinear of lateral

The associate editor coordinating the review of this manuscript and approving it for publication was Bing Li.

forces were considered under various road friction conditions. The proposed observer-based $H\infty$ controller was verified through CarSim® software using a Fishhook maneuver. Peng *et al.* [13] developed an observer-based controller to optimize the performance of a controlled system under an imperfect premise matching condition. Using the practical truck-trailer system, the problem of the original was indicated the usefulness of the proposed observer-based control approach. Du *et al.* [14] proposed a state observer-based T-S fuzzy controller design for a semi-active quarter-car suspension installed with a magneto-rheological (MR) damper. Simulations and tests were conducted on a quarter-car semi-active suspension under various road profiles input. Nguyen *et al.* [15] used a new constrained T-S fuzzy model to design a model-based controller under a large variation range of vehicle speed condition. Extensive simulations and experimental tests were carried out to validate the performance of the proposed method. Jin *et al.* [16] proposed a robust fuzzy controller to improve the stability performance of vehicle lateral dynamic using a T-S fuzzy modeling approach. Simulations with the high-fidelity CarSim® software illustrated the effectiveness of the proposed model-based state-back controller under *J*-turn and Fishhook maneuvers.

Meanwhile, a particular performance constraint control technique was developed in [17] and [18] based on a specially designed prescribed performance function (PPF). Huang *et al.* [19] developed an adaptive prescribed performance function control for vehicle active suspension to stabilize the vertical and pitch motions, and the transient and steady-state suspension response is guaranteed in this process. Hua *et al.* [20] designed a novel prescribed performance control strategy to deal with unknown dead-zone input and improve the system performances. Simulations are also used to verify the performances of the designed control scheme.

The methods presented above did not consider the variations of road profile. The nonlinear properties of the tire or the damper characteristics are considered to design the observer and controller to optimize the steady performance of vehicle roll behavior, and the transient performance of vehicle roll behavior is seldom considered. However, since the real road conditions are complex and uncertain, and the accuracy of state estimation, the response of vehicle system and the transient performance of observer-based controller for vehicle roll behavior should be considered under steering wheel input and various road excitation conditions. The main contributions lie in considering the coupling state estimation and transient performance of vehicle roll behavior under various road conditions, as well as the fact that a coupling vehicle roll dynamics using full-car models is proposed to improve the observer-based control's overall performance.

To deal with the above-mentioned issues, this paper considers the following contributions:

- A full-car model-based T-S fuzzy observer is developed to estimate vehicle coupling roll state, and the accuracy of state estimation is verified using CarSim® software.
- The optimal control of observer-based PPF is adopted, and its transient and steady performance is analyzed and compared with traditional model predictive control (MPC) algorithm using CarSim-Matlab® software.

In this paper, a nine degrees of freedom (9-DOFs) full-car model considering vehicle roll coupling dynamics is first developed. Second, a model-based fuzzy observer based on T-S algorithm is used to acquire the higher accuracy of state estimation for vehicle coupling system. Then, a PPF is used to constrain the error transformation of controlled roll behavior state within the prescribed performance boundaries. Based on a sliding mode surface approach, the fuzzy observer and PPF are tuned and utilized to form the observer-based prescribed performance control (PPC) algorithm. Compared with the traditional MPC algorithm, the proposed observer-based control method will further improve the transient performance for vehicle roll behavior under steering wheel input and various road excitation conditions.

The rest of this paper is organized as follows. The vehicle roll, lateral and vertical dynamics models are briefly described in Section II. In Section III, the model-based T-S observer is designed to obtain the accuracy of vehicle roll state under complex driving conditions. In Section IV, the PPC controller based sliding mode surface and PPF is proposed to constrain the roll angle and roll rate within the appropriate range. Section V shows the simulation results of the proposed observer-based PPC algorithm for vehicle roll behavior and a comparison of its control performance with the MPC algorithm under the same driving conditions in CarSim-Matlab® software. Section VI presents the final conclusions.

II. VEHICLE DYNAMICS MODELLING

In this section, a full-car dynamic model along with T-S model for the identification of both nonlinear tire force and MR damper force are presented.

A. FULL-CAR DYNAMICS MODELING

To further illustrate the practical vehicle driving condition, a 9-DOFs full-car model is established based on the following assumptions [4], as shown in Fig. 1.

1) Effect of slip between the tires and road surface was ignored, and longitudinal acceleration of the vehicle was not considered.
2) Effect of the air force was excluded.
3) Effect of the steering system was ignored.
4) Suspension in steering wheel alignment parameters was ignored.

The 9-DOFs model includes of lateral, vertical and roll dynamics model utilized to illustrate yaw motion, lateral motion, vertical motion and roll motion. Table 1 describes the symbols used in Fig. 1, and the corresponding vehicle parameters originate from CarSim® (D-Class, SUV) [21], [22].

Furthermore, the three-dimensional (3-D) road roughness with straight driving condition and steering working condi-

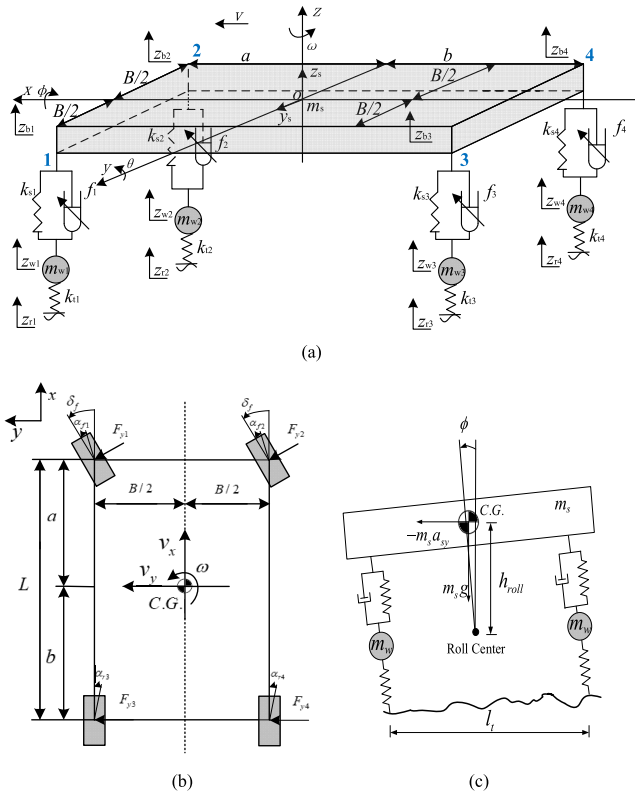

FIGURE 1. 9-DOFs vehicle dynamics model. (a) Full-car model (b) Lateral model (c) Roll model.

TABLE 1. Symbols used for 9-DOFs full-car model.

Vehicle model parameters	Symbol & Unit	Value	Source
Distance from center of gravity (C.G.) to front axle	a / m	1.05	Measurement
Distance from C.G. to rear axle	b / m	1.569	Measurement
Steering angle of front left side	δ_{fl} / (°)	--	Calculation
Steering angle of front right side	δ_{fr} / (°)	--	Calculation
Displacement of the front/rear axle	l_t / m	1.565	Measurement
Suspension stiffness	k_{si} / N/m	34000	Measurement
Tire stiffness	k_{ti} / N/m	230000	Measurement
Sprung mass of vehicle body	m_s / kg	1429	Measurement
Unsprung mass	m_{wi} / kg	40	Measurement
Suspension damping coefficient	f_i / Ns/m	--	Calculation
Sprung mass distance of C.G.	z_b / m	--	Calculation
Sprung mass distance	z_{bi} / m	--	Calculation
Unsprung mass distance	z_{wi} / m	--	Calculation
Road profile	z_{ri} / m	--	Calculation
Distance between roll center to C.G. of sprung mass	h_{roll} / m	0.5	Measurement
longitudinal acceleration of C.G.	a_x / m/s^2	--	Calculation
lateral acceleration of C.G.	a_y / m/s^2	--	Calculation
vertical acceleration of C.G.	a_z / m/s^2	--	Measurement
Roll angle	ϕ / (°)	--	Calculation
Roll rate	$\dot{\phi}$ / (°/s)	--	Measurement
Pitch angle	θ / (°)	--	Calculation

tion are used in this paper. Refer to [8] for a more detailed description of the 3-D road roughness.

According to Table 1, $i = 1, 2, 3, 4$ represents left front side, right front side, left rear side and right rear side for the vehicle system, respectively.

To further illustrate the relationship among different parts of the full-car system, the frame of earth-fixed inertial coordinate and vehicle-fixed non-inertial coordinate should be established to describe the translation of sprung mass center of C.G., the unsprung mass C.G. and rotations of the C.G. of unsprung mass. Refer to [4], [23], and [24] for the detailed corresponding equations.

Using Newton's second law, the 9-DOFs model can be expressed as follows.

Vehicle sprung mass vertical motion:

$$F_s = \sum_{i=1}^{4} F_{si} = -m_s \ddot{z}_b \tag{1}$$

where F_s is the total suspension force. Corresponding equations can be obtained as follows.

$$\begin{aligned} F_{s1} &= -k_{s1}(z_{b1} - z_{w1}) - f_1; \\ F_{s2} &= -k_{s2}(z_{b2} - z_{w2}) - f_2; \\ F_{s3} &= -k_{s3}(z_{b3} - z_{w3}) - f_3; \\ F_{s4} &= -k_{s4}(z_{b4} - z_{w4}) - f_4; \end{aligned} \tag{2}$$

And,

$$\begin{aligned} z_{b1} &= z_b + \frac{B}{2}\sin\phi - a\sin\theta; \\ z_{b2} &= z_b - \frac{B}{2}\sin\phi - a\sin\theta; \\ z_{b3} &= z_b + \frac{B}{2}\sin\phi + b\sin\theta; \\ z_{b4} &= z_b - \frac{B}{2}\sin\phi + b\sin\theta; \end{aligned} \tag{3}$$

Unsprung mass vertical motion:

$$\begin{aligned} m_{w1}\ddot{z}_{w1} &= -k_{s1}(z_{w1} - z_{b1}) - f_1 - k_{t1}(z_{w1} - z_{r1}); \\ m_{w2}\ddot{z}_{w2} &= -k_{s2}(z_{w2} - z_{b2}) - f_2 - k_{t2}(z_{w2} - z_{r2}); \\ m_{w3}\ddot{z}_{w3} &= -k_{s3}(z_{w3} - z_{b3}) - f_3 - k_{t3}(z_{w3} - z_{r3}); \\ m_{w4}\ddot{z}_{w4} &= -k_{s4}(z_{w4} - z_{b4}) - f_4 - k_{t4}(z_{w4} - z_{r4}); \end{aligned} \tag{4}$$

Vehicle sprung mass pitch motion:

$$M_y = \sum_{i=1}^{4} M_{yi} = I_y\ddot{\theta} = (F_{s1} + F_{s2})a - (F_{s3} + F_{s4})b + m_s g h_{roll}\sin\theta \tag{5}$$

where M_y, $i = 1, 2, 3, 4$ is vehicle pitch moment.

Vehicle sprung mass roll motion:

$$M_x = \sum_{i=1}^{4} M_{xi} = I_x\ddot{\phi} = (F_{s2} + F_{s4})\frac{B}{2} - (F_{s1} + F_{s3})\frac{B}{2} + m_s h_{roll}(g\sin\theta + a_{sy}) \tag{6}$$

where M_x, $i = 1, 2, 3, 4$ is vehicle roll moment.

Vehicle lateral motion:

$$F_y = \sum_{i=1}^{4} F_{yi} = m_s a_{sy} + \sum_{i=1}^{4} m_{wi} a_{wyi} = (F_{y1} + F_{y2})\cos\delta_f + (F_{y3} + F_{y4})\cos\delta_r; \tag{7}$$

where F_y, $i = 1, 2, 3, 4$ is tire lateral force. The vehicle lateral force can be calculated using the Magic Formula (MF), more details can be obtained in [23].

Eq. (8) for the vehicle yaw motion:

$$\begin{aligned} M_z = \sum_{i=1}^{4} M_{zi} = I_z\dot{\omega} = b(F_{y3} + F_{y4})\cos\delta_r \\ - a(F_{y1} + F_{y2})\cos\delta_f \\ - B/2(F_{y2} - F_{y1})\sin\delta_r - B/2(F_{y4} + F_{y3})\sin\delta_f \\ + M_{zz1} + M_{zz2} + M_{zz3} + M_{zz4} \end{aligned} \quad (8)$$

where M_{zzi}, $i = 1, 2, 3, 4$ is tire self-aligning moment.

B. REPRESENTATION FOR T-S FULL-CAR VEHICLE MODEL

Firstly, the MF tire model cannot work well since it depends on many nonlinearities that should be known under various parameters situation. Therefore, a T-S fuzzy approach of the tire model is proposed to describe the nonlinearities of the tire lateral forces. The T-S fuzzy rules state the following:

$$\text{If } |\alpha| \text{ is } \mathrm{M}_1, \quad \text{then } \begin{cases} F_{yf} = C_{f1}\alpha_f \\ F_{yr} = C_{r1}\alpha_r \end{cases} \quad (9)$$

$$\text{If } |\alpha| \text{ is } \mathrm{M}_2, \quad \text{then } \begin{cases} F_{yf} = C_{f2}\alpha_f \\ F_{yr} = C_{r2}\alpha_r \end{cases} \quad (10)$$

where C_{fi}, C_{ri} are the front and rear tire cornering stiffness; α_{f}, α_{r} are the front and rear tire slip angle; M_1, M_2 are the small and large fuzzy set for slip angle.

Remark: The Pacejka tire model (a nonlinear model) indicates the relationship between cornering forces and slip angle, as shown in Fig. 2 [23] Since both α_{f} and α_{r} have similar values, the proposed fuzzy rules are only applied for α_{f}.

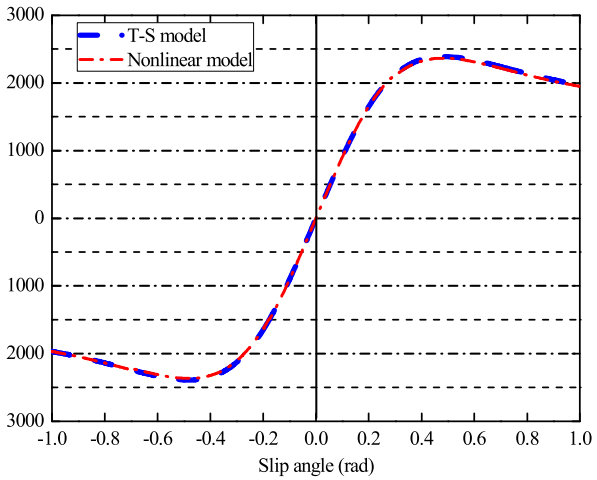

FIGURE 2. Comparison results of T-S and nonlinear lateral tire model.

Based on the vehicle theory and T-S fuzzy approach, the overall lateral forces are given by:

$$\begin{aligned} F_{yf} &= \mu_1\left(|\alpha_f|\right) C_{f1}\alpha_f + \mu_2\left(|\alpha_f|\right) C_{f2}\alpha_f \\ F_{yr} &= \mu_1\left(|\alpha_f|\right) C_{\mathrm{r}1}\alpha_r + \mu_2\left(|\alpha_f|\right) C_{r2}\alpha_r \end{aligned} \quad (11)$$

where μ_{j} $(j = 1, 2)$ is the jth bell curve membership function of fuzzy set $M\mathrm{j}$ that satisfies the following properties:

$$\sum_{i=1}^{2} \mu_i\left(|\alpha_f|\right) = 1; \quad 0 \le \mu_i\left(|\alpha_f|\right) \le 1; \; i = 1, 2 \quad (12)$$

The expressions of the membership functions used are:

$$\mu_i\left(|\alpha_f|\right) = \frac{\varsigma_{\mathrm{i}}\left(|\alpha_f|\right)}{\sum_{i=1}^{2} \varsigma_i\left(|\alpha_f|\right)}; \quad i = 1, 2 \quad (13)$$

And

$$\varsigma_{\mathrm{i}}\left(|\alpha_f|\right) = \frac{1}{\left(1 + \left|\left(\left(|\alpha_f| - c_i\right)/a_i\right)\right|\right)^{2bi}} \quad (14)$$

where a_{i}, b_{i}, c_{i}, C_{fi}, and C_{ri} $(i = 1, 2)$ are identified using the Levenberg–Marquardt algorithm [25]. More details are given in Table 2.

TABLE 2. Model parameters of membership functions for T-S lateral tire model.

Parameters	Value	Parameters	Value
a_1	0.109	a_2	6.823
b_1	0.071	b_2	23.695
c_1	0.053	c_2	5.639
C_{f1}	86540N/rad	C_{f2}	16357N/rad
C_{r1}	78650N/rad	C_{r2}	17250N/rad

The nonlinear lateral tire force by T-S rules, and the nonlinear full-car model can be described by the using T-S fuzzy model. Based on the mentioned above, the nonlinear tire lateral force can be calculated and compared with the MF tire model. Results show that, under large slip angle, the T-S vehicle model has a better computation accuracy as shown in Fig. 2. Refer to [8] and [25] for more details about T-S tire modeling.

Secondly, the dynamic properties of an MR damper are further tested with an MTS machine (Test Rig Model: 850; MTS Systems Corporation). The different corresponding currents are chosen to energize the magnetic field with the same sinusoidal movement routine (with 20 mm amplitude and max 0.2m/s velocity). Fig. 3 shows the force-velocity relationships of the MR damper varying the input voltage.

Based on the above test data and suspension dynamics, the force-velocity phenomenological of the MR damper through the Bouc-Wen model, and the corresponding nonlinear functions can be obtained as follows.

$$\begin{aligned} f_{1i} &= c_{ob}(\dot{z}_{\mathrm{b}i} - \dot{z}_{wi}) + a_b z_{ri}; \\ f_{2i} &= -|z_{ri}|\left[\gamma\,|\dot{z}_{\mathrm{b}i} - \dot{z}_{wi}| - \beta(\dot{z}_{\mathrm{b}i} - \dot{z}_{wi})\mathrm{sign}(z_{ri})\right]; \end{aligned} \quad (15)$$

Since the state variables z_{bi}, $z_{\mathrm{w}1}$, and z_{ri} are limited in practice, the nonlinear functions $f_{1\mathrm{i}}$ and $f_{2\mathrm{i}}$ are also bounded. To deal with $f_{1\mathrm{i}}$ and $f_{2\mathrm{i}}$, the use of T-S fuzzy modeling

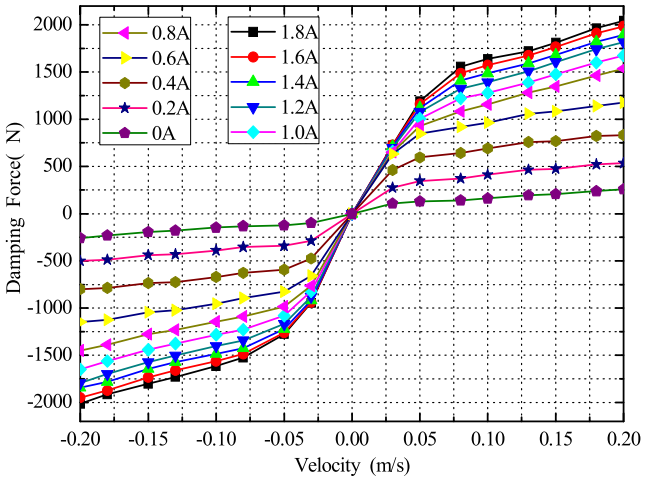

FIGURE 3. Force-velocity map of the MR damper.

approach [26] is convenient to describe the nonlinear system. More details are given in the following.

$$f_{1i} = M_{1i} f_{1i\max} + M_{2i} f_{1i\min};$$
$$f_{2i} = N_{1i} f_{2i\max} + N_{2i} f_{2i\min}; \quad (16)$$

where M_{1i}, M_{2i}, N_{1i} and N_{2i} are fuzzy membership functions, and $\sum_{j=1}^{2}\sum_{i=1}^{4} M_{ji} = 1 \sum_{j=1}^{2}\sum_{i=1}^{4} N_{ji} = 1$. $f_{\max}$ and $f_{\min}$ represent the upper bound and lower bound of the nonlinear force f, the four membership functions are defined as.

$$M_{1i} = \frac{c_{ob}(\dot{z}_{bi} - \dot{z}_{wi}) + a_b z_{ri} - f_{1i\min}}{f_{1i\max} - f_{1i\min}};$$
$$M_{2i} = 1 - M_{1i};$$
$$N_{1i} = \frac{-|z_{ri}|\left[\gamma\,|\dot{z}_{bi} - \dot{z}_{wi}| - \beta(z_{bi} - z_{wi})\mathrm{sign}(z_{ri})\right] - f_{2imix}}{f_{2i\max} - f_{2i\min}};$$
$$N_{2i} = 1 - N_{1i}; \quad (17)$$

Then, the original damper force can be described by the four linear equations, and each damper force can be described using the IF…THEN… logic conditional statement. Then, the T-S fuzzy approach of the damper force could be described with the following equations:

$$\begin{aligned}
&\text{If } f_1 \text{ is } M_1 \textit{ and } f_2 \text{ is } N_1, \quad \text{Then } f_i = f_{11} + f_{21};\\
&\text{If } f_1 \text{ is } M_1 \textit{ and } f_2 \text{ is } N_2, \quad \text{Then } f_i = f_{11} + f_{22};\\
&\text{If } f_1 \text{ is } M_2 \textit{ and } f_2 \text{ is } N_1, \quad \text{Then } f_i = f_{12} + f_{21};\\
&\text{If } f_1 \text{ is } M_2 \textit{ and } f_2 \text{ is } N_2, \quad \text{Then } f_i = f_{12} + f_{22}; \quad (18)
\end{aligned}$$

Based on this analysis, the T-S models for tire modeling and MR damper modeling are used to form the full-car T-S dynamics model. For further details see [12], [14], and [27].

III. STATE ESTIMATION FOR T-S FULL-CAR MODEL

This section aims to obtain the coupled roll angle and roll rate under steering input and various road excitation conditions. The structure of the model-based observer is shown in Fig. 4.

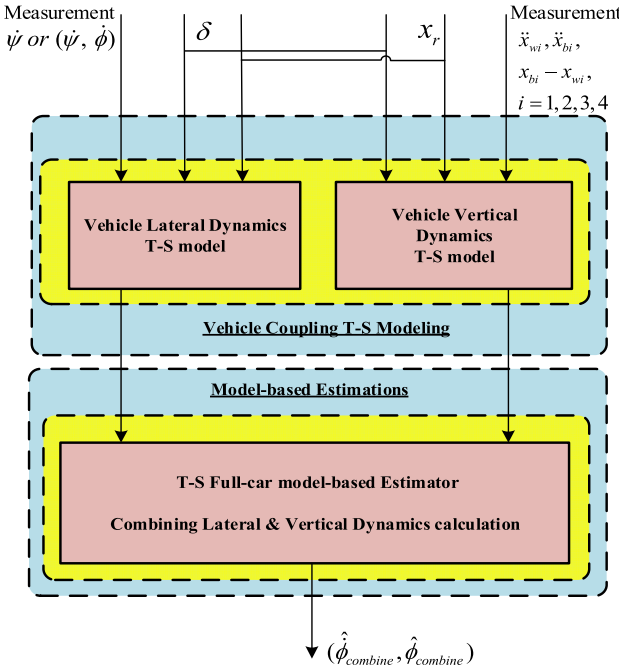

FIGURE 4. Flow chart of T-S model-based observer.

For the T-S observer design for lateral and vertical dynamics, δ and x_r are the system input; then, a T-S model-based observer for the estimation of the roll angle and roll rate is developed as follows.

$$\dot{\hat{\mathbf{x}}}(t) = \sum_{i=1}^{4} \mu_i\left(|\hat{\alpha}_f|\right)\left(\mathbf{A}_i\hat{\mathbf{x}}(t) + \mathbf{B}_i u(t) + \mathbf{L}_i(\mathbf{y}(t) - \hat{\mathbf{y}}(t))\right)$$
$$\hat{\mathbf{y}}(t) = \mathbf{C}\hat{\mathbf{x}}(t) \quad (19)$$

where

$$\hat{\boldsymbol{x}} = [v_y, \omega, \phi, \dot{z}_b, \dot{\theta}, \dot{\phi}, z_{bi} - z_{wi}, \dot{z}_{wi}, z_{wi} - z_{ri}]^T;$$
$$\boldsymbol{u} = [\delta, f_1, f_2, f_3, f_4]^T;$$
$$\hat{\boldsymbol{y}} = [\ddot{z}_b, \omega, \dot{\theta}, \dot{\phi}, \ddot{z}_{wi}]^T; \quad i = 1, 2, 3, 4$$

where $\boldsymbol{x}$ is the state estimation vector of the model, and $\boldsymbol{y}$ represents the output matrix. By using measurable signals, the roll state can be estimated. Appendix A gives the details of $\mathbf{A}_i$ and $\mathbf{B}_i$ matrixes

Using measurable signals, e.g., the steering wheel angle and sprung mass acceleration, the roll angle and roll rate can be estimated with Eq. (19). The aim of the design is to determine gain matrices $\boldsymbol{L}_i$, which guarantee the asymptotic convergence of $\hat{\mathbf{x}}(t)$ to $\mathbf{x}(t)$. The state estimation error is defined as follows.

$$\mathbf{e}(t) = \mathbf{x}(t) - \hat{\mathbf{x}}(t) \quad (20)$$

The dynamics of state estimation error is obtained as follows.

$$\dot{\mathbf{e}}(t) = \sum_{i=1}^{2}\sum_{j=1}^{2} \mu_i\left(|\hat{\alpha}_f|\right)\mu_j\left(|\alpha_f|\right)((\mathbf{A}_i - \mathbf{L}_i C)e(t) + \Delta\mathbf{A}_{ij}x(t) + \Delta\mathbf{B}_{ij}\delta(t)) + \mathbf{B}_w\phi_r(t) \quad (21)$$

And

$$\Delta \mathbf{A}_{ij} = \mathbf{A}_j - \mathbf{A}_i; \quad \Delta \mathbf{B}_{ij} = \mathbf{B}_j - \mathbf{B}_i \tag{22}$$

Defining:

$$\mathbf{x}_e(t) = \begin{bmatrix} e(t) \\ x(t) \end{bmatrix}, \quad \mathbf{w} = \begin{bmatrix} \delta(t) \\ \phi_r(t) \end{bmatrix} \tag{23}$$

The augmented system calculated from (17) and state estimation error (18) can be calculated as follows

$$\dot{\mathbf{x}}_e(t) = \sum_{i=1}^{2} \sum_{j=1}^{2} \mu_i \left(\left| \hat{\alpha}_f \right| \right) \mu_j \left(\left| \alpha_f \right| \right) \left(\tilde{\mathbf{A}}_{ij} e(t) + \tilde{\mathbf{B}}_{ij} w(t) \right) \tag{24}$$

where

$$\tilde{\mathbf{A}}_{ij} = \begin{bmatrix} \mathbf{A}_i - \mathbf{L}_i \mathbf{C} & \Delta \mathbf{A}_{ij} \\ 0 & \mathbf{A}_j \end{bmatrix}; \quad \tilde{\mathbf{B}}_{ij} = \begin{bmatrix} \Delta \mathbf{B}_{ij} & \mathbf{B}_w \\ \mathbf{B}_j & \mathbf{B}_w \end{bmatrix} \tag{25}$$

Remark: Because disturbances $\boldsymbol{w}(t)$ is composed of the steering angle input and the various road profiles, it can be logically considered to have finite energy [22].

The gains $\boldsymbol{L}_i$ has been calculated by considering the effect of the road profile on the state estimation errors. One possible approach is to minimize the $\boldsymbol{L}_2$ gain from disturbances to the estimation errors. The relationship of $\boldsymbol{L}_2$ gain between $\boldsymbol{w}(t)$ and $\boldsymbol{e}(t)$ can be defined as follows [12], [25]

$$\gamma = \sup \frac{\|e(t)\|}{\|w(t)\|} \tag{26}$$

By setting the supremum and the $\boldsymbol{L}_2$ gain, Eq. (26) can be expressed as follows

$$\int_0^\infty e(t)^T e(t) dt \leq \gamma^2 \int_0^\infty w(t)^T w(t) dt \tag{27}$$

Theorem 1: If there exist positive and symmetric matrices $\mathbf{P}_1$ and $\mathbf{P}_2$, matrices $\mathbf{M}_\mathrm{i}$ and positive scalar γ satisfying the following linear matrix inequalities (LMI) for $i, j = 1, 2$.

$$\begin{bmatrix} \mathbf{\Theta}_\mathrm{i} & \mathbf{P}_1 \Delta A_{ij} & \mathbf{P}_1 \Delta \mathbf{B}_{ij} & \mathbf{P}_1 \mathbf{B}_w \\ \Delta \mathbf{A}_{ij}^T \mathbf{P}_1 & \mathbf{\Psi}_j & \mathbf{P}_2 \mathbf{B}_j & \mathbf{P}_2 \mathbf{B}_w \\ \Delta \mathbf{B}_{ij}^T \mathbf{P}_1 & \mathbf{B}_J^T \mathbf{P}_2 & -\gamma^2 \mathbf{I} & 0 \\ \mathbf{B}_w^T \mathbf{P}_1 & \mathbf{B}_w^T \mathbf{P}_2 & 0 & -\gamma^2 \mathbf{I} \end{bmatrix} < 0; \tag{28}$$

where

$$\begin{aligned} \mathbf{\Theta}_i &= \mathbf{A}_i^T \mathbf{P}_1 + \mathbf{P}_1 \mathbf{A}_i - \mathbf{M}_i \mathbf{C} - \mathbf{C}^T \mathbf{M}_i^T + \mathbf{I}; \\ \mathbf{\Psi}_j &= \mathbf{A}_j^T \mathbf{P}_2 + \mathbf{P}_2 \mathbf{A}_j \end{aligned} \tag{29}$$

Then, the vector $\boldsymbol{e}(t)$ converges asymptotically to desire value. The gains of the observer are given by $\mathbf{L}_i = \mathbf{P}_1^{-1} \mathbf{M}_i$. The corresponding proof for observer stability and LMI condition in ***Theorem* 1** are presented in Appendix B and Appendix C. Further details can be found in [12], [28], and [29]

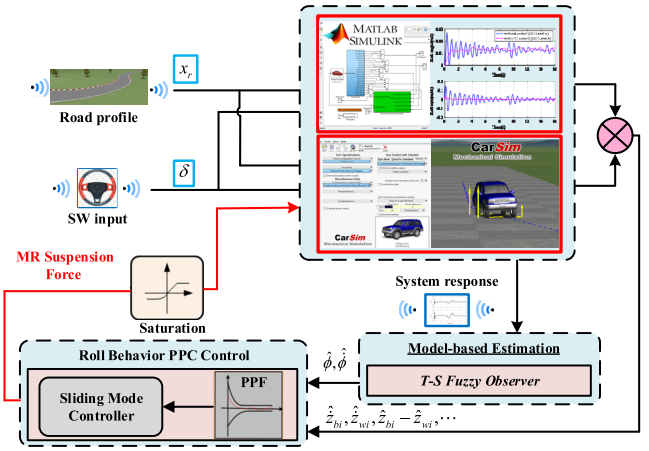

FIGURE 5. Flow chart of the observer-based control algorithm.

IV. OBSERVER-BASED CONTROL FOR T-S FULL-CAR MODEL

In this section, an observer-based optimal control is proposed for vertical and lateral dynamics to constraint the roll motion; the structure of the controller is shown in Fig. 5. For applying PPC algorithm, the prescribed performance function (PPF) is first produced, that is, an error transformation function is adapted to integrate the performance constraints of vehicle suspension system into the following controller design. Then, based on the PPF, the sliding mode surface is used to form the PPC approach. The process of tuning the PPC under various road excitations and steering wheel input is further elaborated in the following sections

A. ERROR TRANSFORMATION WITH PPF

Due to considering safety and hardware limitations of semi-active suspension, the following performance and structure requirements are considered (30) and (31)

1) The input saturation of semi-active suspension control force, defined as:

$$sat\ (u_i) = \begin{cases} u_{max\,i}, & if\ u_i > u_{max\,i} \\ u_i, & if\ -u_{max\,i} \leq u_i \leq u_{max\,i} \\ -u_{max\,i}, & if\ u_i < -u_{max\,i} \end{cases} \tag{30}$$

where sat (u_i) represents saturation function.

2) The vertical displacement and roll angle can be attenuated using the damping force.
3) The movement of mechanical structure can be constrained as follows.

$$\begin{aligned} |\Delta x_{b1}| &= \left| x_b + \frac{l_t}{2} \cdot sin\ (\phi) - a \cdot sin\ (\theta) - x_{w1} \right| \\ &\leq \Delta x_{b1max}; \\ |\Delta x_{b2}| &= \left| x_b - \frac{l_t}{2} \cdot sin\ (\phi) - a \cdot sin\ (\theta) - x_{w2} \right| \\ &\leq \Delta x_{b2max}; \end{aligned} \tag{31}$$

In this paper, to illustrate a prescribed control bound of roll angle or roll rate, the following positive decreasing function is given (32) and (33) More details can be found in [30] and [31].

$$\varphi_i(t) = (\varphi_{0i} - \varphi_{\infty i})\, e^{-\alpha_i t} + \varphi_{\infty i}, \quad i = 1, 2 \tag{32}$$

where $\varphi_{i\infty}$ is an allowable error in the steady state; $\varphi_i > \varphi_{i\infty}$ are design parameters, and $\lim_{t\to\infty} \varphi(t) = \varphi_{i\infty} > 0$. Note that $i = 1, 2$ denotes the roll angle and roll rate, respectively.

Then, the objective constraints inequation of the prescribed performance can be obtained.

$$-\delta\varphi_i(t) < x_i(t) < \bar{\delta}\varphi_i(t); \quad \forall t > 0 \tag{33}$$

where δ and $\bar{\delta}$ are positive constants used as the constraints. Eq. (33) determines both the transient and steady performance of the controlled state x_i.

Based on the above analysis, to guarantee the performance constraints are always satisfied, the following transformation is proposed.

$$x_i = \varphi_i(t)\, S(z_i) \tag{34}$$

where $S(z_1)$ is a smooth and strictly function.

$$S(z_i) = \frac{\bar{\delta}_i e^{(z_i+v_i)} - \delta_1 e^{-(z_i+v_i)}}{e^{(z_i+v_i)} + e^{-(z_i+v_i)}} \tag{35}$$

where $v_i = \frac{1}{2}\ln\frac{\delta_i}{\bar{\delta}_i}$, and the smooth function $S(z_1)$ has the following properties:

$$\begin{aligned} &1)\ -\delta < S(z_i) < \bar{\delta}; \quad \forall z_1 \in L_\infty \\ &2)\ \lim_{z_i\to+\infty} S(z_i) = \bar{\delta}; \quad \lim_{z_i\to-\infty} S(z_i) = -\bar{\delta}. \\ &3)\ S(0) = 0. \end{aligned} \tag{36}$$

Lemma 1 (34): If the transformed error z_i is bounded, and the initial value of the controlled state $x_i(0)$ is within the performance bounds, i.e., $-\delta\varphi_i(0) < x_i(0) < \bar{\delta}\varphi_i(0)$, then x_i will be maintained within the prescribed performance (36) for all $t \geq 0$ [32].

Because $\varphi(t) \neq 0$, the transformed error z_i can be obtained.

$$z_i = S^{-1}\left[\frac{x_i}{\varphi_i}\right] = S^{-1}(\lambda_i) = \frac{1}{2}\ln\left[\left(\frac{\lambda_i + \delta_i}{\bar{\delta}_i - \lambda_i}\right)\frac{\bar{\delta}_i}{\delta_i}\right] \tag{37}$$

where $\lambda_i = x_i/\varphi$ is transformed error. The derivative of z_i can be obtained as.

$$\dot{z}_i = \frac{\partial S^{-1}}{\partial\lambda_i}\dot{\lambda}_1 = \varpi_i\left(\frac{\dot{x}_i}{\varphi_i} - \frac{x_i\dot{\varphi}_i}{\varphi_i}\right) \tag{38}$$

And

$$\varpi_i = \frac{1}{2}\left[\frac{1}{\lambda_i + \delta_i} - \frac{1}{\lambda_i - \bar{\delta}_i}\right] \tag{39}$$

The second-order time derivative of z_i can be calculated as:

$$\ddot{z}_i = \dot{\varpi}_i\left(\frac{\dot{x}_i}{\varphi_i} - \frac{x_i\dot{\varphi}_i}{\varphi_i}\right) + \varpi_i\left[\ddot{x}_i - \left(\frac{x_i\dot{\varphi}_i + x_i\ddot{\varphi}_i}{\varphi_i} - \frac{x_i\dot{\varphi}^2}{\varphi_i^2}\right)\right] \tag{40}$$

B. ADAPTIVE PPC FEEDBACK CONTROL DESIGN

In this section, according to ***Lemma* 1**, the PPF bound should be achieved. To achieve this control purpose and consider transient and steady performance improvement, the sliding mode surface is defined as.

$$s_i = [\Lambda_i, 1]\,[z_i, \dot{z}_i] \tag{41}$$

where $\Lambda_i > 0$ is a positive constant such that z_i is bounded as long as s_i is bounded [29].

Then, to further illustrate the PPC approach, z_1 (roll angle) is used as an objective. More details are given as follows.

According to (41), the time derivative of s_1 is given as.

$$\begin{aligned} \dot{s}_1 = \Lambda_1\dot{\phi} + \ddot{\phi} = {} & \Lambda_1\dot{\phi} + a_1(z_{b1} - z_{w1}) + a_2(z_{b2} - z_{w2}) \\ & + a_3\dot{z}_b + a_4\dot{z}_{w1} + a_5\dot{z}_{w2} + a_6\phi + a_7\dot{\phi} + U_\phi \end{aligned} \tag{42}$$

And

$$\begin{aligned} a_1 &= \frac{B\cdot k_{s1}}{2\left(I_x + m_s\cdot h_{roll}^2\right)}; \quad a_2 = \frac{-B\cdot k_{s1}}{2\left(I_x + m_s\cdot h_{roll}^2\right)}; \\ a_3 &= 0; \quad a_4 = \frac{-c_1}{2\left(I_x + m_s\cdot h_{roll}^2\right)}; \\ a_5 &= \frac{c_1}{2\left(I_x + m_s\cdot h_{roll}^2\right)}; \quad a_6 = \frac{m_s\cdot h_{roll}\cdot g}{I_x + m_s\cdot h_{roll}^2}; \\ a_7 &= \frac{-B^2\cdot c_1}{2\left(I_x + m_s\cdot h_{roll}^2\right)}; \end{aligned}$$

where U_φ represents the input force of the suspension system.

Based on particle swarm optimization algorithm, Eq. (42) can be expressed as.

$$\dot{s}_1 = \Lambda_1\dot{\phi} + \ddot{\phi} = \Lambda x_7 + W_1^T\Phi_1 + \varepsilon_{01} \tag{43}$$

And,

$$\begin{aligned} W_1 &= \left[\omega_1^T, 1\right]^T (\|W_1\| \leq W_{1N}); \quad \Phi_1 = \left[\phi_1^T(z_1), U_\phi\right]^T; \\ \omega_1^T\phi_1 &= a_1(z_{b1} - z_{w1}) + a_2(z_{b2} - z_{w2}) + a_3\dot{z}_b + a_4\dot{z}_{w1} \\ &\quad + a_5\dot{z}_{w2} + a_6\phi + a_7\dot{\phi}; \end{aligned}$$

where ε_{01} is residual error function, i.e. $|\varepsilon_{01}| \leq \varepsilon_{01N} = 0$, w_1^T is augmented weight, φ_1 is the regressor.

Based on the adaptive control method, U_φ can be calculated as follows:

$$U_\phi = -\hat{\omega}_1^T\phi_1(z_1) - k_1 s_1 - \Lambda_1\dot{\phi}_1 \tag{44}$$

where $k_1 > 0$ is feedback gain;$\hat{\omega}_1$ is estimation parameter of ω_1, and the adaptive control law updates in real time.

Also, by substituting (44) into (42).

$$\dot{s}_1 = -k_1 s_1 + \tilde{W}_1^T\Phi_1 + \varepsilon_{01} \tag{45}$$

where the $\tilde{W}_1$ is adaptive control law. The method of reducing order is used to solve $\tilde{W}_1$, and more details are given as follows.

The method of reducing order is calculated using tracking error, and Eq. (46) can be given,

$$\dot{\tilde{W}}_1 = \Gamma_1 s_1\Phi_1 - \Gamma_1\sigma H_1 \tag{46}$$

Being,

$$H_1 = \mathbf{P}_1\tilde{W}_1 - Q_1; \quad \dot{P}_1 = -lP_1 + \Phi_1\Phi_1^T;$$
$$\dot{Q}_1 = -lQ_1 + \Phi_1(s_1/k)$$

where $\Gamma_1 > 0$ is adaptive gain; $\sigma > 0$ is a constant; $k > 0$ and $l > 0$ are positive constants; $P_1(0)$ and $Q(0)$ are equal to zero.

Based on the above adaptive control law $\tilde{W}_1$ and suspension force U_φ, the control error of roll angle asymptotically converges to the presetting range under no residual error condition.

Proof: Design the following Lyapunov candidate as:

$$V_1 = \frac{1}{2}s_1^2 + \frac{1}{2}\tilde{W}_1^T\Gamma_1^{-1}\tilde{W}_1 \tag{47}$$

Take the derivative of V_1:

$$\begin{aligned}\dot{V}_1 &= -k_1s_1^2 + s_1\varepsilon_{01} - \sigma\tilde{W}_1^TP_1\tilde{W}_1 + \sigma\tilde{W}_1^T\Delta_1\\ &\le -\left(k_1 - \frac{1}{2\eta_1}\right)s_1^2 - \sigma\left(\sigma_1 - \frac{1}{2\eta_1}\right)\left\|\tilde{W}_1\right\|^2\\ &\quad + \frac{\eta_1}{2}\left(\varepsilon_{1N}^2 + \sigma\varepsilon_{1Nf}^2\right)\\ &\le -\tilde{\mu}_1V_1 + \gamma_1\end{aligned} \tag{48}$$

where $\tilde{\mu}_1 = \min\{2(k_1 - 1/2\eta_1),\ 2\sigma\Gamma_1(\sigma_1 - 1/2\eta_1)/\lambda_{\max}\}$ and $\gamma_1 = \eta_1(\varepsilon_{1N}^2 + \sigma\varepsilon_{1Nf}^2)/2$ are all positive constants, and $k_1 > 1/2\eta_1$, $\eta_1 > 1/2\sigma_1$. The detailed verification can be found in [29]. Then, using Barbalat Lemma [19], s_1 and $\tilde{W}_1$ converge to the sets defined.

Without considering the MR time delay and the interrupted effect of road profile, the modified anti-windup technique is used to tackle the control saturation when the MR suffers from input constraints [33]. The core of anti-windup modification is to design an augmented controller, and the obtained new controller should have the corresponding characters as follow [29], [33]. This method can be easily expressed by low order structures [34], and it can be written as follows.

$$\dot{\vartheta}_1 = -\chi_0\vartheta_1 + \zeta_0\rho_1 + \xi_0\Delta F \tag{49}$$

where χ_0, ξ_0, $\zeta 0$, ρ_1 are positive constants; $F = U_\varphi\text{-sat}(U_\varphi)$ with sat(.) as the saturation function [34].

Then, Eq. (44) can be rewritten as:

$$U_\phi = -\hat{\omega}_1^T\phi_1(z_1) - k_1s_1 - \Lambda_1\dot{\phi}_1 + \chi_0\vartheta_1 \tag{50}$$

Note that χ_0 is used to compensate the error s_1 when $F \neq 0$. When the input is very small, then, χ_0 is also zero, and the stability of the studied system is saved. When saturation occurs, θ_1 can reshape U_φ to make the controller back into the linear region of the saturation.

Proof: Design the Lyapunov candidate as:

$$V_1' = \frac{1}{2}s_1^2 + \frac{1}{2}\tilde{W}_1^T\Gamma_1^{-1}\tilde{W}_1 + \frac{1}{2}\vartheta_1^2 \tag{51}$$

Then, the time derivative of V_1' can be computed as:

$$\begin{aligned}\dot{V}_1' &= -k_1's_1^2 + s_1\varepsilon_{01} + k_0\eta_1s_1 - \sigma\tilde{W}_1^TP_1\tilde{W}_1 + \sigma\tilde{W}_1^T\Delta_1\\ &\quad + \eta_1(-k_0\eta_1 + \theta_0\Delta F)\\ &\le -\left(k_1' - \frac{1}{2\eta_{sc1}} - \frac{k_0}{2\eta_{sc1}}\right)s_1^2 - \sigma\left(\sigma_1 - \frac{k_0}{2\eta_{sc1}}\right)\left\|\tilde{W}_1\right\|^2\\ &\quad - \left(k_0 - \frac{k_0\eta_{sc1}}{2} - \frac{1}{2\eta_{sc1}}\right)\eta_1^2\\ &\quad + \frac{k_0\eta_{sc1}}{2}(\varepsilon_{1N}^2 + \sigma\varepsilon_{1Nf}^2 + (\theta_0\Delta F)^2)\\ &\le -\tilde{\mu}_1'V_1' + \gamma_1'\end{aligned} \tag{52}$$

where $\tilde{\mu}_1' = \min\{2(k_1' - 1/2\eta_1 - k_0/2\eta_{sc1}),\ 2\sigma(\sigma_1 - 1/2\eta_1),\ 2(k_0 - k_0\eta_{sc1}/2 - 1/2\eta_1)\}$, $\gamma_1 = \eta_{sc1}(\varepsilon_{1N}^2 + \sigma\varepsilon_{1Nf}^2(\theta_0F)^2)/2$ are all positive constants, $k_1' > 1/2\eta_1 + k_0/2\eta_{sc1}$, $\eta_{sc1} > 1/2\sigma_1$, and $k_0 > 1/(2\eta_{sc1} - \eta_{sc1}^2)$. The continuity of the saturation function validated that the set of $\Omega_1(s_1,\ \tilde{\mu_1}',\ \eta_1)$ can be defined to be larger than Ω_2, i.e., $\Omega_2 \in \Omega_1$. Then, the control error s_1 is still bounded [30].

V. MPC STRATEGIES

As an optimal control approach, MPC is used to calculate the optimization problem of the studied system. The general system model is given as follows [35], [36]

$$\begin{cases}x_*(k+1) = A_*(k)x(k) + B_*(k)u_*(k) + n_*(k)\\ y_*(k) = C_*(k)x(k) + D_*(k)u_*(k) + v_*(k)\end{cases} \tag{53}$$

where $x*(k)$ represents states, $u*(k)$ is control inputs, $y*(k)$ represents the outputs, $n*(k)$ represents the state noise and $v*(k)$ represents the measurement noise.

An objective function is proposed to illustrate both the reference tracking error and the control effort. The corresponding function can be defined to obtain the optimal objective as follows.

$$\begin{aligned}\min_{u_0,u_1,\ldots,u_{N-1}} J &= \min_{u_0,u_1,\ldots,u_{N-1}} \sum_{i=1}^{M-1}\\ &\times\begin{bmatrix} w_{i+1}^y \left\|y(k+i+1\,|k\,) - y_{ref}(k+i+1\,|k\,)\right\|^2\\ +w_i^u\left\|u(k+i+1\,|k\,)\right\|^2\end{bmatrix}\end{aligned} \tag{54}$$

$$\begin{aligned}\text{s.t. } y_{min} \le y(k) \le y_{max}, \quad k = 0, 1, \ldots M-1\\ u_{min} \le u(k) \le u_{max}, \quad k = 0, 1, \ldots M-1\end{aligned} \tag{55}$$

where M represents the prediction length; w^{u} and w^{y} represent the weights for the control input u and the output y.

VI. SIMULATION AND VALIDATION

The proposed T-S estimation and PPC algorithm were validated using industrial standard simulation software. A standard SUV vehicle model established in CarSim® (Version 8.0.2) software was utilized together with Matlab® (2016) to form simulator as shown in Fig. 5 [37], [38].

A. SIMULATION AND VALIDATION

The PPC Simulation was run under steering wheel (SW) input varying the road excitation conditions, and the results were compared with those of the MPC algorithm [35], [36]. Table I gives the vehicle simulation parameters while Table 3 and Fig. 6 provide the simulation situation and controller settings.

TABLE 3. Simulation setting of vehicle roll behavior control.

Parameters	Descriptions or Values
Road profile of setting with PPC & MPC	ISO-*A*, ISO-*C*
Steering wheel input of PPC & MPC setting	45°
Classification interval of PPC & MPC setting	0.001s
Vehicle velocity of PPC & MPC setting	40km/h
Algorithm validation time	16s
Initial system state $\boldsymbol{x}$ of MPC setting	$\boldsymbol{x}$=zeros(9, 1);
Prediction steps (N_p) of MPC setting	10
Control steps (N_c) of MPC setting	8
Solve MPC weight matrix ($\boldsymbol{R}$, $\boldsymbol{Q}$)	$\boldsymbol{R}$=Diag(2e-8*N_c); $\boldsymbol{Q}$=$\boldsymbol{G}$'*$\boldsymbol{G}$+$\boldsymbol{R}$;
Note: $\boldsymbol{G}$ matrix is composed of system matrix $\boldsymbol{A}$, $\boldsymbol{B}$, $\boldsymbol{C}$. More details in [46].	

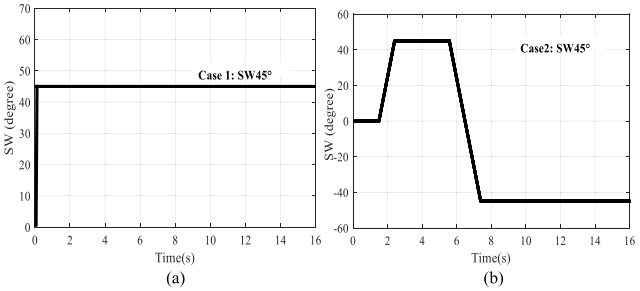

FIGURE 6. Simulation of vehicle roll under various driving situations. (a) *J*-turn (b) Fishhook.

Due to the physical limitation of the suspension actuators, the input constraints limits for the external suspension force were set to 2000N. The following observer gains in (30) were chosen: $\varphi_{01} = \varphi_{02} = 0.6$, $\varphi_{\infty 1} = 0.018$, $\varphi_{\infty 2} = 0.01$, $\alpha_1 = 1.1$, and $\alpha_2 = 1$ in the J-turn simulation, and $\varphi_{01} = \varphi_{02} = 0.6$, $\varphi_{\infty 1} = 0.01$, $\varphi_{\infty 2} = 0.01$, $\alpha_1 = 1.1$ and $\alpha_2 = 1.1$ in the Fishhook simulation. A certain tolerance on the lateral offset is desired to prevent the lateral slip or rollover. So, for the roll angle and roll rate, are set to $\delta_1 = \bar{\delta}_1 = 0.1$ and $\delta_2 = \bar{\delta}_2 = 0.15$ under the various conditions. For the adaptive control algorithm, $k_1 = 68$, $\Gamma_1 = 0.02$. To alleviate the chattering effect, the saturation function with a boundary layer 0.01 is used to reliance the sign function in the simulation for proposed control [4], [20]. Note that the road ISO level *A*/*C* excitation can be generated using the Power Spectral Density (PSD) method. See [40]–[44] for further details.

B. SIMULATION RESULTS

The observer-based PPC control strategy proposed in Section 4 was used to improve the roll behavior performance of the vehicle system under various driving conditions. Due to tire hop, the errors of state estimation and control performance would grow under the varying road levels [45]–[47]. To further explain how the PPF and MPC algorithms affect the effective control of the vehicle system, the performance of control algorithms were validated.

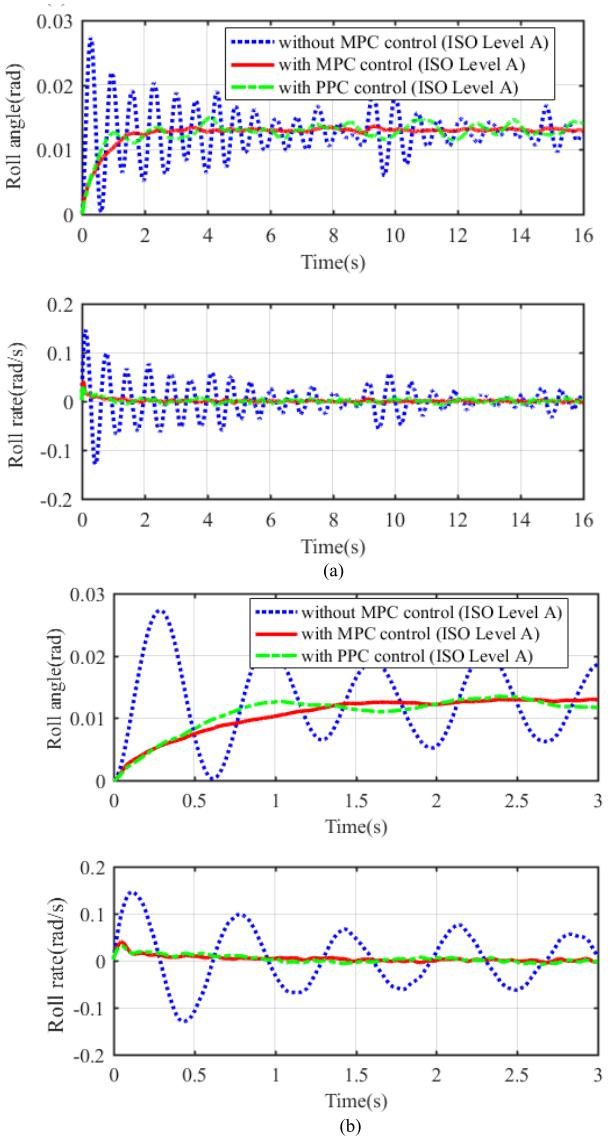

FIGURE 7. Control results of ISO-A road and SW 45° (J-turn simulation). (a) simulation results from 0 to 16 seconds, (b) simulation results from 0 to 3 seconds.

Case 1 (J-Turn Simulation): In this section, using the vehicle dynamics model and the observer-based control algorithm, the vehicle roll performance was calculated under road ISO level *A*/*C* excitation as shown in Figs. 7 and 8

Figs. 7 and 8 show the results of PPC and MPC algorithms controlled under SW 45° input and ISO-*A* road excitation conditions, respectively. Furthermore, the time segment corresponding to the 16 (3) simulation second in Fig. 7a (b) (i.e. from $t = 0$ second to $t = 16$ (3) second) is plotted for the *J*-turn simulation under road ISO Level-*A* excitation.

According to Fig. 7, no matter which control algorithm is used, a relatively good control effect is obtained. For the MPC algorithm, the transient response time of improving control is no longer than two seconds, and the steady performance of the vehicle system is also achieved two seconds later.

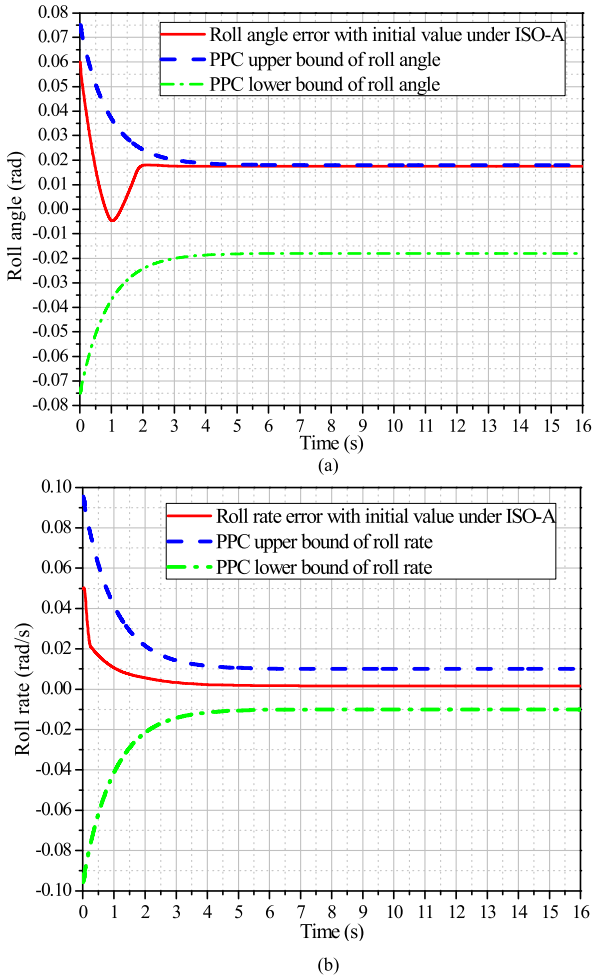

FIGURE 8. PPC control of roll state under ISO-A road and SW 45° conditions (*J*-turn simulation). (a) Roll angle (b) Roll rate.

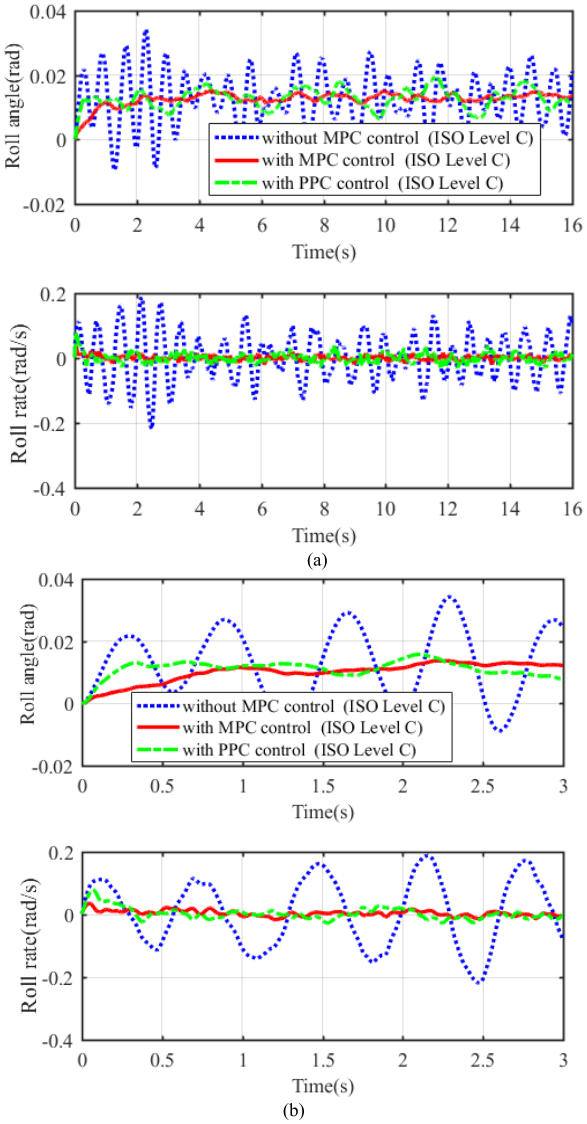

FIGURE 9. Control results for ISO-*C* road profile and SW 45° (*J*-turn simulation). (a) simulation results from 0 to 16 seconds, (b) simulation results from 0 to 3 seconds.

Also, the steady value of MPC approach does not fluctuate very much. For the PPC algorithm, the corresponding output response of improving transient performance of vehicle roll behavior is better than that of MPC approach, then the restricted effect on roll stability can be adaptively weakened. However, the steady response of PPC algorithm is less than MPC algorithm two seconds later under ISO-*A* and SW input condition. That is because the primary control objective of PPC algorithm is constrained in prescribed performance bounds, and the secondary goal is to ensure the roll performance. Then, the PPC approach is the optimal constrained range, and is not the optimum value optimization in real time.

To further illustrate the control performance of the PPC approach, the corresponding transient and steady response were simulated under the ISO-*C* road excitation as shown in Figs. 9 and 10. In Fig. 9a (b), the time segment corresponding to the 16 (3) simulation second (i.e. from t = second to t = 16 (3) second) is plotted for the *J*-turn simulation under road ISO Level-*C* excitation. Fig. 9 shows the steady and transient response values of fluctuating characteristic of vehicle roll behavior are higher than those of ISO-*A* road excitation. However, for the PPC and MPC algorithms, the control effect is noticeable, i.e., they both can obtain satisfactory steady performance for vehicle roll behavior under ISO-*C* and SW input condition. Also, in Fig. 7 and Fig. 9, different road excitation impacts significantly on roll behavior, and the influence of road excitation cannot be ignored [48]–[50].

Overall, when the PPC and MPC algorithms work under the various driving conditions, the roll stability performance of the vehicle system can be significantly improved in the *J*-turn simulation.

Case 2 (Fishhook Simulation): Based on the Fishhook simulation, as shown in Figs. 11-14, the roll response of using PPC algorithm in Fishhook condition was computed under ISO level *A*/*C* road excitation. In Fig. 11a (b), the time segment corresponding to the 16 (10) simulation second (i.e., from t = 0 second to t = 16 (10) second) is plotted for the Fishhook simulation under road ISO Level-*A* excitation.

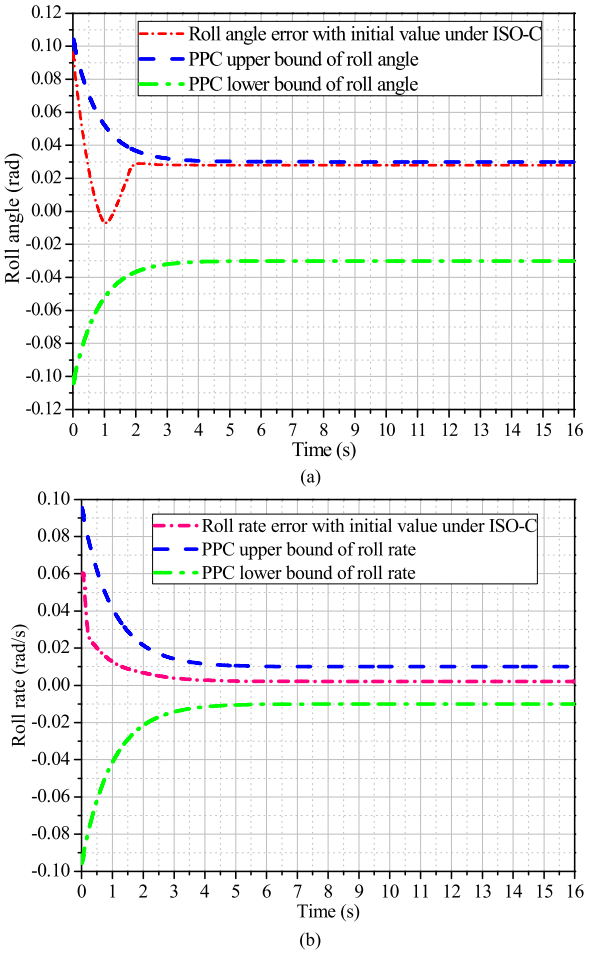

FIGURE 10. PPC control of roll state under ISO-C road and SW 45° conditions (*J*-turn simulation). (a) Roll angle (b) Roll rate.

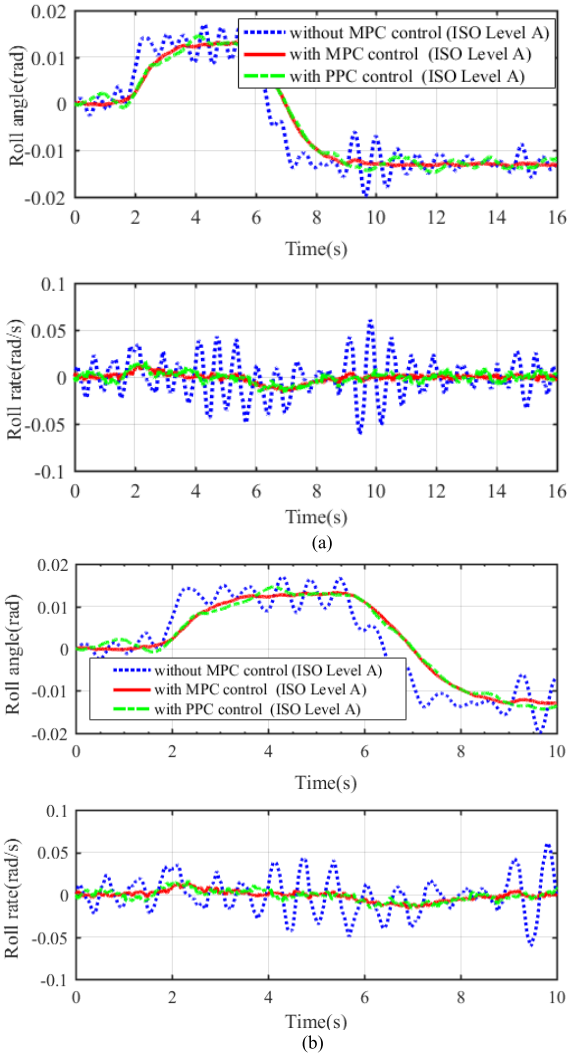

FIGURE 11. Control results for ISO-A road profile and SW 45° (Fishhook simulation). (a) simulation results from 0 to 16 seconds, (b) simulation results from 0 to 10 seconds.

In Fig. 13a (b), the time segment corresponding to the 16 (10) simulation second (i.e., from $t = 0$ second to $t = 16$ (10) second) is plotted for the Fishhook simulation under road ISO Level-*C* excitation.

As previously explained, when the vehicle is changing the lane with high speed, the input and output signals change dramatically in a very short period. To guarantee the roll stability, it is reasonable and necessary to tolerate a larger steady-state error.

From Fig. 12, the controlled roll state are all well restricted in the prescribed performance bounds, with small overshoots and steady-state errors. Some errors still exist in the controlled states during the lane-change maneuver [34]. Therefore, the proposed control can effectively reduce the overshoots in these states, and restrict them in safe boundaries. In the steady state, their values are similar with different control strategies, and the performance is visible, i.e., they can obtain a good steady performance for vehicle roll behavior under ISO-*A* and SW input condition. The response of transient and steady were also simulated under the ISO-*C* road excitation as shown in Fig. 13 and Fig. 14.

TABLE 4. Calculation STD error of T-S fuzzy observer various on road level-*A*/*C* profile at 40km/h.

Simulation condition	Filter state estimation	Road level excitation	Compared data	Simulation & Validation results STD_error(%)
J-turn	Roll angle	Level ISO-*A*	T-S estimated and CarSim® simulation data	10.6
		Level ISO-*C*		12.4
	Roll rate	Level ISO-*A*		8.9
		Level ISO-*C*		9.5
Fishhook	Roll angle	Level ISO-*A*		12.8
		Level ISO-*C*		15.7
	Roll rate	Level ISO-*A*		10.6
		Level ISO-*C*		11.6

Similar results can be obtained for ISO-C road excitation. Meanwhile, the steady and transient response value of fluctuating characteristic of vehicle roll behavior under road ISO-*C* excitation is also higher than that of ISO-*A* road excitation. Also, the oscillations on control inputs in the initial phase are

TABLE 5. Calculation RMS values of PPC control various on road level-*A*/*C* profiles at 40 km/h.

Simulation condition	Controlled roll state	Road level excitation	RMS value of uncontrolled input	RMS value of controlled input	Improvement accuracy of comparing controlled & uncontrolled / %
J-turn	Roll angle	Level ISO-*A*	0.0135	0.0127	5.93%
		Level ISO-*C*	0.0153	0.0128	16.3%
	Roll rate	Level ISO-*A*	0.0318	0.0035	88.9%
		Level ISO-*C*	0.0744	0.0076	89.7%
Fishhook	Roll angle	Level ISO-*A*	0.0119	0.0113	5.04%
		Level ISO-*C*	0.0138	0.0113	18.1%
	Roll rate	Level ISO-*A*	0.0191	0.0046	75.9%
		Level ISO-*C*	0.0667	0.0082	87.7%

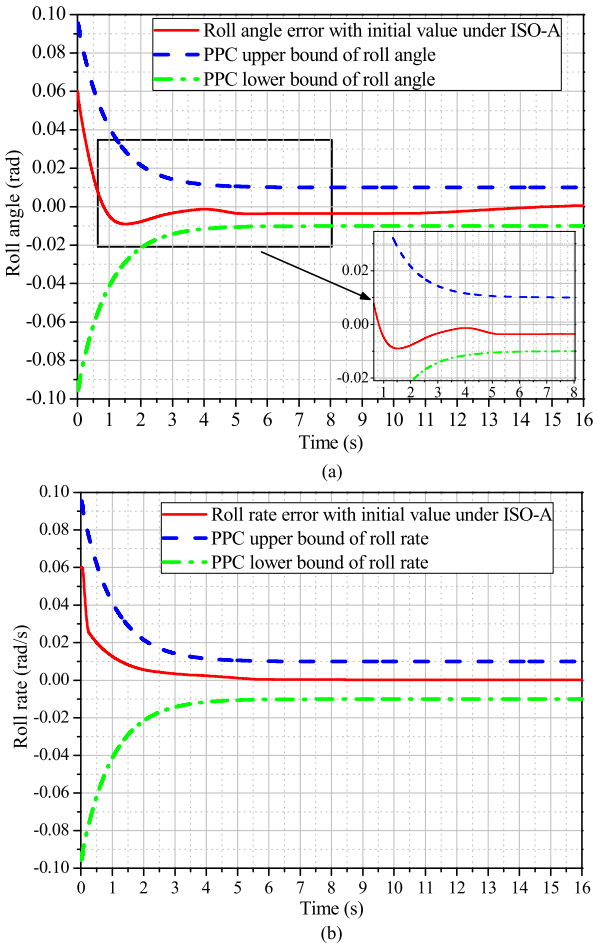

FIGURE 12. PPC control of roll state under ISO-A road excitation and SW 45° conditions (Fishhook simulation). (a) Roll angle (b) Roll rate.

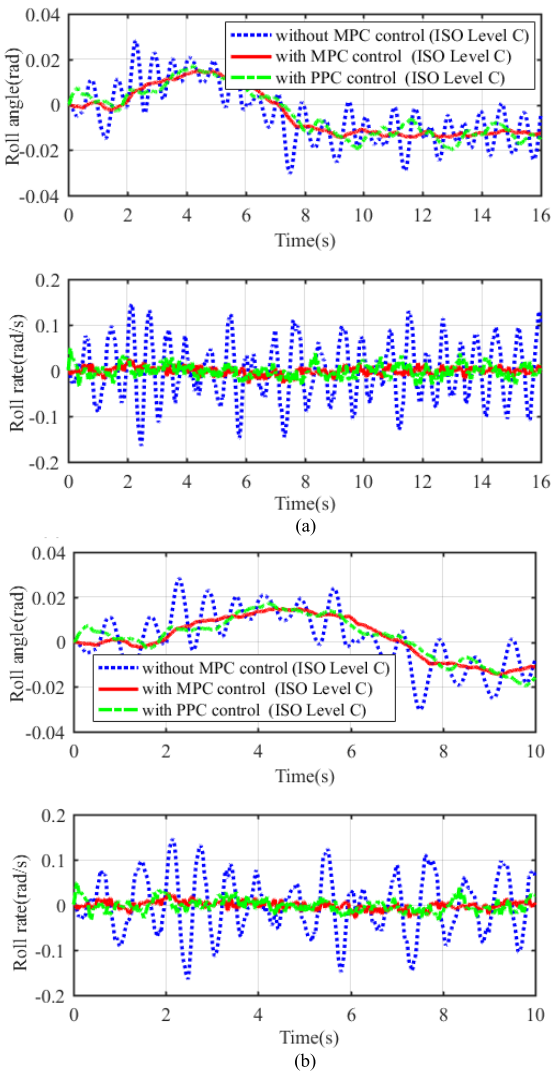

FIGURE 13. Control results of ISO-C road and SW 45° (Fishhook simulation). (a) simulation results from 0 to 16 seconds, (b) simulation results from 0 to 10 seconds.

caused by the strict prescribed performance control requirements, which therefore is reasonable.

Based on the T-S model-based fuzzy observer analysis, the error values of the estimation standard deviation (STD) were calculated under ISO Level-*A*/*C* road excitation, and the results of the comparison are given in Table 4.

Table 4 shows that the performance (RMS-error) change stays within 16% in all the relevant signals. The values of the control and uncontrolled root mean square (RMS) are also calculated, and the simulation results of the uncontrolled situation, MPC algorithm and PPC algorithm are summarized in Table 5.

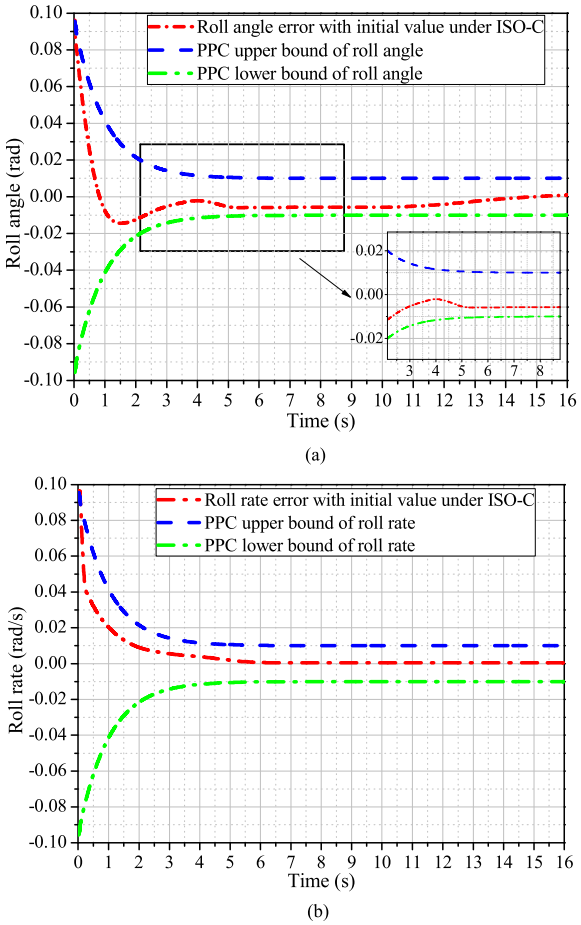

FIGURE 14. PPC control of roll state under ISO-C road excitation and SW 45° conditions (Fishhook simulation). (a) Roll angle (b) Roll rate.

VII. CONCLUSIONS

In this paper, the optimal control of vehicle roll under SW input and various road excitation was studied using 9-DOFs full-car model. Then, with the proposed observer-based control algorithm, the influence of the full-car model on vehicle roll behavior was studied.

The following main conclusions can be drawn:

(1) A full-car T-S model and model-based T-S fuzzy observer were developed under various SW input and road excitation conditions and the LMI theory was then used to illustrate the stability of T-S fuzzy observer.

(2) Compared to the MPC algorithm and uncontrolled situations, the proposed PPC algorithm could better improve the transient and steady performance of vehicle roll behavior under various external excitations in real time.

Finally, simulation results showed that the proposed observer-based PPC algorithm could improve the performance of roll behavior for a vehicle system, and was validated in CarSim-Matlab® under various driving situations and different road excitation levels.

In the future, the proposed control algorithm will be used with a practical full-car. Also, further research will extend to pattern recognition optimization control for a 9-DOFs vehicle system and focus on the application of corresponding data for developing intelligent vehicles.

APPENDIX A

Based on the T-S full-car model, the responses of system matrixes $\mathbf{A_i}$ and $\mathbf{B}_i$ stated in (19) are as follows.

$$\mathbf{A}_i = \begin{bmatrix} \mathbf{A}_{11} & \mathbf{A}_{12} & \mathbf{A}_{13} \\ \mathbf{A}_{21} & \mathbf{A}_{22} & \mathbf{A}_{23} \\ \mathbf{A}_{31} & \mathbf{A}_{32} & \mathbf{A}_{33} \end{bmatrix};$$

$$\mathbf{A}_{11} = \begin{bmatrix} A'_{11} & A'_{12} & 0 & 0 & 0 & 0 \\ A'_{21} & A'_{22} & 0 & 0 & 0 & 0 \\ 0 & 0 & 0 & 0 & 0 & 1 \\ 0 & 0 & 0 & A'_{44} & A'_{45} & 0 \\ 0 & 0 & 0 & A'_{54} & A'_{55} & 0 \\ A'_{61} & A'_{62} & A'_{63} & 0 & 0 & A'_{66} \end{bmatrix};$$

$$\mathbf{A}_{12} = \begin{bmatrix} 0 & 0 & 0 & 0 & 0 & 0 \\ 0 & 0 & 0 & 0 & 0 & 0 \\ 0 & 0 & 0 & 0 & 0 & 0 \\ A'_{47} & A'_{48} & A'_{49} & A'_{410} & A'_{411} & A'_{412} \\ A'_{57} & A'_{58} & A'_{59} & A'_{510} & A'_{511} & A'_{512} \\ A'_{67} & A'_{68} & A'_{69} & A'_{610} & A'_{611} & A'_{612} \end{bmatrix};$$

$$\mathbf{A}_{13} = \begin{bmatrix} 0 & 0 & 0 & 0 & 0 & 0 \\ 0 & 0 & 0 & 0 & 0 & 0 \\ 0 & 0 & 0 & 0 & 0 & 0 \\ A'_{413} & A'_{413} & 0 & 0 & 0 & 0 \\ A'_{513} & A'_{514} & 0 & 0 & 0 & 0 \\ A'_{613} & A'_{614} & 0 & 0 & 0 & 0 \end{bmatrix};$$

$$\mathbf{B}_2 = \begin{bmatrix} 0 & 0 & 0 & 0 & 0 & 0 \\ 0 & 0 & 0 & 0 & \frac{1}{m_{w1}} & 0 \\ 0 & 0 & 0 & 0 & 0 & \frac{1}{m_{w2}} \\ 0 & 0 & 0 & 0 & 0 & 0 \\ 0 & 0 & 0 & 0 & 0 & 0 \end{bmatrix};$$

$$\mathbf{B}_3 = \begin{bmatrix} 0 & 0 & 0 & 0 & 0 & 0 \\ 0 & 0 & 0 & 0 & 0 & 0 \\ 0 & 0 & 0 & 0 & 0 & 0 \\ \frac{1}{m_{w3}} & 0 & 0 & 0 & 0 & 0 \\ 0 & \frac{1}{m_{w4}} & 0 & 0 & 0 & 0 \end{bmatrix};$$

$$\mathbf{A}_{21} = \begin{bmatrix} 0 & 0 & 0 & 1 & -a & \frac{l_t}{2} \\ 0 & 0 & 0 & 1 & -a & -\frac{l_t}{2} \\ 0 & 0 & 0 & 1 & b & \frac{l_t}{2} \\ 0 & 0 & 0 & 1 & b & -\frac{l_t}{2} \\ 0 & 0 & 0 & \frac{f_1}{m_{w1}} & -\frac{f_1 \cdot a}{m_{w1}} & \frac{f_1 \cdot l_t}{2 \cdot m_{w1}} \\ 0 & 0 & 0 & \frac{f_2}{m_{w2}} & -\frac{f_2 \cdot a}{m_{w2}} & -\frac{f_2 \cdot l_t}{2 \cdot m_{w2}} \end{bmatrix};$$

$$\mathbf{A}_{22}=\begin{bmatrix} 0 & 0 & 0 & 0 & -1 & 0 \\ 0 & 0 & 0 & 0 & -1 & 0 \\ 0 & 0 & 0 & 0 & -1 & 0 \\ 0 & 0 & 0 & 0 & -1 & 0 \\ \frac{k_s}{m_{w1}} & 0 & 0 & 0 & 0 & 0 \\ 0 & 0 & 0 & 0 & 0 & -\frac{f_2}{m_{w2}} \end{bmatrix};$$

$$\mathbf{A}_{23}=\begin{bmatrix} 0 & 0 & 0 & 0 & 0 & 0 \\ 0 & 0 & 0 & 0 & 0 & 0 \\ 0 & 0 & 0 & 0 & 0 & 0 \\ 0 & 0 & 0 & 0 & 0 & 0 \\ 0 & 0 & -\frac{k_t}{m_{w1}} & 0 & 0 & 0 \\ 0 & 0 & 0 & -\frac{k_t}{m_{w2}} & 0 & 0 \end{bmatrix};$$

$$\mathbf{A}_{31}=\begin{bmatrix} 0 & 0 & 0 & \frac{f_3}{m_{w3}} & \frac{f_3\cdot b}{m_{w3}} & \frac{f_3\cdot l_t}{2\cdot m_{w3}} \\ 0 & 0 & 0 & \frac{f_4}{m_{w4}} & \frac{f_4\cdot b}{m_{w4}} & -\frac{f_4\cdot l_t}{2\cdot m_{w4}} \\ 0 & 0 & 0 & 0 & 0 & 0 \\ 0 & 0 & 0 & 0 & 0 & 0 \\ 0 & 0 & 0 & 0 & 0 & 0 \\ 0 & 0 & 0 & 0 & 0 & 0 \end{bmatrix};$$

$$\mathbf{A}_{32}=\begin{bmatrix} 0 & 0 & 0 & \frac{k_s}{m_{w3}} & 0 & 0 \\ 0 & 0 & 0 & 0 & \frac{k_s}{m_{w4}} & 0 \\ 0 & 0 & 0 & 0 & 1 & 1 \\ 0 & 0 & 0 & 0 & 1 & 1 \\ 0 & 0 & 0 & 0 & 1 & 1 \\ 0 & 0 & 0 & 0 & 1 & 1 \end{bmatrix};$$

$$\mathbf{A}_{33}=\begin{bmatrix} -\frac{f_3}{m_{w3}} & 0 & 0 & 0 & -\frac{k_t}{m_{w3}} & 0 \\ 0 & -\frac{f_4}{m_{w4}} & 0 & 0 & 0 & -\frac{k_t}{m_{w4}} \\ 1 & 1 & 0 & 0 & 0 & 0 \\ 1 & 1 & 0 & 0 & 0 & 0 \\ 1 & 1 & 0 & 0 & 0 & 0 \\ 1 & 1 & 0 & 0 & 0 & 0 \end{bmatrix};$$

$$A'_{11}=\frac{\sigma'_i\cdot I'_{xeq}}{M\cdot I_x\cdot v_x};\quad A'_{12}=\frac{\rho'_i\cdot I'_{xeq}}{M_1\cdot I_x\cdot v_x}-v_x;\ A'_{21}=\frac{\rho'_i}{I_z};$$

$$A'_{22}=\frac{-\tau'_i}{I_z v_x};\quad A'_{44}=-\frac{4\cdot f}{m_s};\ A'_{45}=\frac{2\cdot a\cdot f-2\cdot b\cdot f}{m_s};$$

$$A'_{47}=-\frac{k_s}{m_s};\quad A'_{48}=-\frac{k_s}{m_s};\ A'_{49}=-\frac{k_s}{m_s};\ A'_{410}=-\frac{k_s}{m_s};$$

$$A'_{411}=\frac{f}{m_s};\quad A'_{412}=\frac{f}{m_s};\ A'_{413}=\frac{f}{m_s};\ A'_{414}=\frac{f}{m_s};$$

$$A'_{54}=\frac{2\cdot a\cdot f-2\cdot b\cdot f}{I_y};\quad A'_{55}=-\frac{2\cdot a^2\cdot f+2\cdot b^2\cdot f}{I_y};$$

$$A'_{57}=\frac{a\cdot k_s}{I_y};\quad A'_{58}=\frac{a\cdot k_s}{I_y};\ A'_{59}=-\frac{b\cdot k_s}{I_y};\ A'_{510}=-\frac{b\cdot k_s}{I_y};$$

$$A'_{511}=-\frac{a\cdot f}{I_y};\quad A'_{512}=-\frac{a\cdot f}{I_y};\ A'_{513}=\frac{b\cdot f}{I_y};$$

$$A'_{514}=\frac{b\cdot f}{I_y};\quad A'_{61}=\frac{-m_s\cdot h_{roll}\cdot\sigma'_i}{M_1 I_x};\ A'_{62}=\frac{m_s\cdot h_{roll}\cdot\rho'_i}{M_1 I_x v};$$

$$A'_{63}=\frac{m_s\cdot g\cdot h_{roll}-h_{roll}\cdot K_\phi}{I_x};\quad A'_{66}=\frac{-h_{roll}\cdot C_\phi-l_t^2\cdot f}{I_x};$$

$$A'_{67}=-\frac{l_t\cdot k_s}{2I_x};\quad A'_{68}=\frac{l_t\cdot k_s}{2I_x};\ A'_{69}=-\frac{l_t\cdot k_s}{2I_x};$$

$$A'_{610}=\frac{l_t\cdot k_s}{2I_x};\quad A'_{611}=\frac{l_t\cdot f}{2I_x};\ A'_{612}=-\frac{l_t\cdot f}{2I_x};$$

$$A'_{613}=\frac{l_t\cdot f}{2I_x};\quad A'_{614}=-\frac{l_t\cdot f}{2I_x};$$

and

$$\sigma'_i=2(C_{fi}+C_{ri});\quad \rho'_i=2(bC_{ri}-aC_{fi}cos(\delta_f));$$

$$\tau'_i=2(a^2C_{fi}\cos(\delta_f)+b^2C_{ri});\quad I'_{xeq}=m_s h_{roll}^2+I_x^2;$$

$$\mathbf{B}_i=\begin{bmatrix}\mathbf{B}_1 & \mathbf{B}_2 & \mathbf{B}_3\end{bmatrix};$$

$$\mathbf{B}_1=\begin{bmatrix} \frac{2\cdot C_{fi}\cdot C_{ri}}{M} & \frac{2\cdot C_{fi}\cdot a}{I_z} & 0 & 0 & \frac{2\cdot m_s\cdot h_{roll}\cdot C_{fi}}{M\cdot(I_x+m_s\cdot h_{roll}^2)} & 0 \\ 0 & 0 & 0 & \frac{-1}{m_s} & \frac{a}{I_y} & \frac{-l_t}{2\cdot(I_x+m_s\cdot h_{roll}^2)} \\ 0 & 0 & 0 & \frac{-1}{m_s} & \frac{a}{I_y} & \frac{l_t}{2\cdot(I_x+m_s\cdot h_{roll}^2)} \\ 0 & 0 & 0 & \frac{-1}{m_s} & \frac{-b}{I_y} & \frac{-l_t}{2\cdot(I_x+m_s\cdot h_{roll}^2)} \\ 0 & 0 & 0 & \frac{-1}{m_s} & \frac{-b}{I_y} & \frac{l_t}{2\cdot(I_x+m_s\cdot h_{roll}^2)} \end{bmatrix}.$$

APPENDIX B

The corresponding proof for observer stability and LMI condition in ***Theorem* 1** are as follows.

Proof: When we assume the following Lyapunov function condition:

$$V(\mathbf{x}_e)=\mathbf{x}_e(t)^T\mathbf{P}\mathbf{x}_e(t) \tag{B1}$$

With $\boldsymbol{P}=\boldsymbol{P}^{\mathrm{T}}>0$. The state estimation error $\boldsymbol{e}(t)$ can be defined as follows:

$$\mathbf{e}(t)=\mathbf{C}_e\mathbf{x}_e(t) \tag{B2}$$

And,

$$\mathbf{C}_e=[\mathbf{I}\quad 0] \tag{B3}$$

System (22) is stable and the H_∞ gain of the transfer from $\boldsymbol{w}(t)$ to $\boldsymbol{e}(t)$ is bounded by $\gamma>0$ if the following inequation satisfies:

$$\mathbf{J}_\infty=\dot{\mathbf{V}}(\mathbf{x}_e)+\mathbf{e}(t)^{\mathrm{T}}\mathbf{e}(t)-\gamma^2\mathbf{w}(t)^{\mathrm{T}}\mathbf{w}(t)<0 \tag{B4}$$

Substituting Eq. (22) into Eq. (B4) yields:

$$\sum_{i=1}^{2}\sum_{j=1}^{2}\mu_i(|\hat{\alpha}_f|)\mu_i(|\alpha_f|)(\mathbf{x}_e(t)^{\mathrm{T}}\tilde{\mathbf{A}}_{ij}^T\mathbf{P}\mathbf{x}_e(t)+\mathbf{x}_e(t)^T\mathbf{P}\tilde{A}_{ij}\mathbf{x}_e(t))$$
$$+\mathbf{w}(t)^T\tilde{\mathbf{B}}_{ij}^T\mathbf{P}\mathbf{x}_e(t)+\mathbf{x}_e(t)^T\mathbf{P}\tilde{\mathbf{B}}_{ij}\mathbf{w}(t)+\mathbf{x}_e(t)^T\mathbf{x}_e(t)$$
$$-\gamma^2\mathbf{w}(t)^T\mathbf{w}(t)<0 \tag{B5}$$

Eq. (B5) can be rewritten as follows:

$$\sum_{i=1}^{2}\sum_{j=1}^{2}\mu_i(|\hat{\alpha}_f|)\mu_i(|\alpha_f|)\begin{bmatrix}\mathbf{x}_e\\ \mathbf{w}\end{bmatrix}^T\begin{bmatrix}\mathbf{Y}_{ij} & \mathbf{P}\tilde{\mathbf{B}}_{ij}\\ \tilde{\mathbf{B}}_{ij}^T\mathbf{P} & -\gamma^2\mathbf{I}\end{bmatrix}\begin{bmatrix}\mathbf{x}_e\\ \mathbf{w}\end{bmatrix}<0 \tag{B6}$$

where

$$\mathbf{Y}_{ij}=\tilde{\mathbf{A}}_{ij}^T\mathbf{P}+\mathbf{P}\tilde{\mathbf{A}}_{ij}+\mathbf{C}_e^T\mathbf{C}_e \tag{B7}$$

According to the convex sum property of the activation functions, Eq. (B6) can be satisfied if the following inequation is satisfied:

$$\begin{bmatrix}\mathbf{Y}_{ij} & \mathbf{P}\tilde{\mathbf{B}}_{ij}\\ \tilde{\mathbf{B}}_{ij}^T\mathbf{P} & -\gamma^2\mathbf{I}\end{bmatrix}<0,\quad \forall i,j=1,2. \tag{B8}$$

These constrains are nonlinear. To obtain LMI conditions, the following particular form of matrix $\mathbf{P}$ is considered:

$$\mathbf{P}=\begin{bmatrix}\mathbf{P}_1 & 0\\ 0 & \mathbf{P}_2\end{bmatrix} \tag{B9}$$

Substituting Eq. (25) and Eq. (B9) into Eq. (B8) yields the following (B10):

$$\begin{bmatrix}\mathbf{\Theta}_{\mathrm{i}} & \mathbf{P}_1\mathbf{\Delta}A_{ij} & \mathbf{P}_1\mathbf{\Delta}\mathbf{B}_{ij} & \mathbf{P}_1\mathbf{B}_w\\ \mathbf{\Delta}\mathbf{A}_{ij}^T\mathbf{P}_1 & \mathbf{\Psi}_j & \mathbf{P}_2\mathbf{B}_j & \mathbf{P}_2\mathbf{B}_w\\ \mathbf{\Delta}\mathbf{B}_{ij}^T\mathbf{P}_1 & \mathbf{B}_J^T\mathbf{P}_2 & -\gamma^2\mathbf{I} & 0\\ \mathbf{B}_w^T\mathbf{P}_1 & \mathbf{B}_w^T\mathbf{P}_2 & 0 & -\gamma^2\mathbf{I}\end{bmatrix}<0; \tag{B10}$$

where

$$\begin{aligned}\mathbf{\Theta}_i&=(\mathbf{A}_i-\mathbf{L}_i\mathbf{C})^T\mathbf{P}_1+\mathbf{P}_1(\mathbf{A}_i-\mathbf{L}_i\mathbf{C})+\mathbf{I};\\ \mathbf{\Psi}_j&=\mathbf{A}_j^T\mathbf{P}_2+\mathbf{P}_2\mathbf{A}_j\end{aligned} \tag{B11}$$

Using variable change $\mathbf{M}_{\mathrm{i}}=\mathbf{P}_1\mathbf{L}_{\mathrm{i}}$, Eq. (B10) is linear in variables $\mathbf{P}_1$, $\mathbf{P}_2$, and $\mathbf{M}_{\mathrm{i}}$, which leads to the equivalent condition calculated by Eq. (28). This suffices to satisfy Eq. (28) and guarantee $\mathbf{V}(t)$ / dt <0 with the γ-attenuation (27).

APPENDIX C

To achieve less-conservative LMI equation of ***Theorem* 1**, the new LMI condition was used to illustrate the stability of the estimation error **e** (t) [51].

Using [52, Th. 2], i.e., if there are matrices $\mathbf{P}_1>0$ and $\mathbf{P}_2>0$, matrices $\mathbf{Q}_{\mathrm{ij}}$, $\mathbf{M}_{\mathrm{j}}$, and scalar γ such that the following LMIs hold:

$$\begin{aligned}&\mathbf{\Gamma}_{ii}+\mathbf{Q}_{ii}<0,\quad i=1,2\\ &\mathbf{\Gamma}_{ij}+\mathbf{\Gamma}_{ji}+\mathbf{Q}_{ij}+\mathbf{Q}_{ji}<0,\quad i<j,\\ &\begin{bmatrix}\mathbf{Q}_{11} & \mathbf{Q}_{12}\\ \mathbf{Q}_{11}^T & \mathbf{Q}_{22}\end{bmatrix}>0,\end{aligned} \tag{C1}$$

With

$$\begin{bmatrix}\mathbf{\Theta}_{\mathrm{i}} & \mathbf{P}_1\mathbf{\Delta}A_{ij} & \mathbf{P}_1\mathbf{\Delta}\mathbf{B}_{ij} & \mathbf{P}_1\mathbf{B}_w\\ \mathbf{\Delta}\mathbf{A}_{ij}^T\mathbf{P}_1 & \mathbf{\Psi}_j & \mathbf{P}_2\mathbf{B}_j & \mathbf{P}_2\mathbf{B}_w\\ \mathbf{\Delta}\mathbf{B}_{ij}^T\mathbf{P}_1 & \mathbf{B}_J^T\mathbf{P}_2 & -\gamma^2\mathbf{I} & 0\\ \mathbf{B}_w^T\mathbf{P}_1 & \mathbf{B}_w^T\mathbf{P}_2 & 0 & -\gamma^2\mathbf{I}\end{bmatrix}<0; \tag{C2}$$

Then, the estimation error **e**(t) is stable and satisfies the $\boldsymbol{L}_2$ gain, i.e., $\mathbf{L}_i=\mathbf{P}_1^{-1}\mathbf{M}_i$

REFERENCES

[1] R. Rajamani, *Vehicle Dynamics and Control*. New York, NY, USA: Springer, 2012, pp. 10–260.

[2] G. Phanomchoeng and R. Rajamani, "New rollover index for the detection of tripped and untripped rollovers," *IEEE Trans. Ind. Electron.*, vol. 60, no. 10, pp. 4726–4736, Oct. 2013.

[3] X. Zhang, Y. Yang, K. Guo, J. Lv, and T. Peng, "Contour line of load transfer ratio for vehicle rollover prediction," *Vehicle Syst. Dyn.*, vol. 55, no. 11, pp. 1748–1763, Apr. 2017.

[4] Z.-F. Wang, M.-M. Dong, L. Gu, J.-J. Rath, Y.-C. Qin, and B. Bai, "Influence of road excitation and steering wheel input on vehicle system dynamic responses," *Appl. Sci.*, vol. 7, no. 6, p. 570, May 2017. doi: 10.3390/app7060570.

[5] A. Riofrio, S. Sanz, M. J. L. Boada, and B. L. Boada, "A LQR-based controller with estimation of road bank for improving vehicle lateral and rollover stability via active suspension," *Sensors*, vol. 17, no. 10, p. 2318, Oct. 2017. doi: 10.3390/s17102318.

[6] J. G. Guzman, L. P. Gonzalez, J. P. Redondo, S. S. Sanchez, and B. L. Boada, "Design of low-cost vehicle roll angle estimator based on Kalman filters and an IoT architecture," *Sensors*, vol. 18, no. 6, p. 1800, Jun. 2018. doi: 10.3390/s18061800.

[7] F. Lu, "Study on vehicle vibration state observation algorithm based on the nonlinearity of suspension," Ph.D. dissertation, Dept. Mech. Eng., Beijing Inst. Technol., Beijing, China, 2014.

[8] C. Hu, R. Wang, F. Yan, Y. Huang, H. Wang, and C. Wei, "Differential steering based yaw stabilization using ISMC for independently actuated electric vehicles," *IEEE Trans. Intell. Transp. Syst.*, vol. 19, no. 2, pp. 627–638, Feb. 2018.

[9] S. E. Li *et al.*, "Dynamical modeling and distributed control of connected and automated vehicles: Challenges and opportunities," *IEEE Intell. Transp. Syst. Mag.*, vol. 9, no. 3, pp. 46–58, Jul. 2017.

[10] M. R. Licea and I. Cervantes, "Robust indirect-defined envelope control for rollover and lateral skid prevention," *Control Eng. Pract.*, vol. 61, pp. 149–162, Apr. 2017.

[11] T. Takagi and M. Sugeno, "Fuzzy identification of systems and its applications to modeling and control," *IEEE Trans. Syst., Man, Cybern. Syst.*, vol. SMC-15, no. 1, pp. 116–132, Jan./Feb. 1985.

[12] H. Dahmani, O. Pagés, A. El Hajjaji, and N. Daraoui, "Observer-based robust control of vehicle dynamics for rollover mitigation in critical situations," *IEEE Trans. Intell. Transp. Syst.*, vol. 15, no. 3, pp. 274–284, Feb. 2014.

[13] C. Peng, S. Ma, and X. Xie, "Observer-based non-PDC control for networked T–S fuzzy systems with an event-triggered communication," *IEEE Trans. Cybern.*, vol. 47, no. 8, pp. 2279–2287, Aug. 2017. doi: 10.1109/TCYB.2017.2659698.

[14] X. Tang, H. Du, S. Sun, D. Ning, Z. Xing, and W. Li, "Takagi–Sugeno fuzzy control for semi-active vehicle suspension with a magnetorheological damper and experimental validation," *IEEE/ASME Trans. Mechatronics*, vol. 22, no. 1, pp. 291–300, Feb. 2017. doi: 10.1109/TMECH.2016.2619361.

[15] A.-T. Nguyen, C. Sentouh, and J.-C. Popieul, "Fuzzy steering control for autonomous vehicles under actuator saturation: Design and experiments," *J. Franklin Inst.*, vol. 355, no. 18, pp. 9374–9395, Dec. 2018. doi: 10.1016/j.jfranklin.2017.11.027.

[16] X. Jin, Z. Yu, G. Yin, and J. Wang, "Improving vehicle handling stability based on combined AFS and DYC system via robust Takagi-Sugeno fuzzy control," *IEEE Trans. Intell. Transp. Syst.*, vol. 19, no. 8, pp. 2696–2707, Aug. 2018. doi: 10.1109/TITS.2017.2754140.

[17] C. P. Bechlioulis and G. A. Rovithakis, "Prescribed performance adaptive control for multi-input multi-output affine in the control nonlinear systems," *IEEE Trans. Autom. Control.*, vol. 55, no. 5, pp. 1220–1226, May 2010.

[18] C. Wang and Y. Lin, "Adaptive dynamic surface control for MIMO nonlinear time-varying systems with prescribed tracking performance," *Int. J. Control*, vol. 88, no. 4, pp. 832–843, Oct. 2015.

[19] Y. Huang, J. Na, X. Wu, and G. Gao, "Approximation-free control for vehicle active suspensions with hydraulic actuator," *IEEE Trans. Ind. Electron.*, vol. 65, no. 9, pp. 7258–7267, Sep. 2018.

[20] C. Hua, J. Chen, Y. Li, and L. Li, "Adaptive prescribed performance control of half-car active suspension system with unknown dead-zone input," *Mech. Syst. Signal Process.*, vol. 111, pp. 135–148, Oct. 2018. doi: 10.1016/j.ymssp.2018.03.048.

[21] D. Tan and C. Lu, "The influence of the magnetic force generated by the in-wheel motor on the vertical and lateral coupling dynamics of electric vehicles," *IEEE Trans. Veh. Technol.*, vol. 65, no. 6, pp. 4655–4658, Jun. 2016.
[22] Z. Wang, M. Dong, Y. Qin , Z. Wang, and T. Xu, "Fuzzy observer for nonlinear vehicle system roll behavior with coupled lateral and vertical dynamics," in *Proc. SAE, Soc. Automot. Eng.*, Troy, MI, USA, 2018. doi: 10.4271/2018-01-0559.
[23] H. Pacejka, *Tire and Vehicle Dynamics*. Oxford, U.K.: Butterworth-Heinemann, 2002, pp. 5–240.
[24] N. Zhang, G.-M. Dong, and H.-P. Du, "Investigation into untripped rollover of light vehicles in the modified fishhook and the sine maneuvers. Part I: Vehicle modelling, roll and yaw instability," *Vehicle Syst. Dyn.*, vol. 46, no. 4, pp. 271–293, Mar. 2008.
[25] H. Dahmani, O. Pagés, and A. El Hajjaji, "Observer-based state feedback control for vehicle chassis stability in critical situations," *IEEE Trans. Control Syst. Technol.*, vol. 24, no. 2, pp. 636–644, Mar. 2016.
[26] H. Li, J. Yu, C. Hilton, and H. Liu, "Adaptive sliding-mode control for nonlinear active suspension vehicle systems using T–S fuzzy approach," *IEEE Trans. Ind. Electron.*, vol. 60, no. 8, pp. 3328–3338, Aug. 2013.
[27] H. Dahmani, M. Chadli, A. Rabhi, and A. EI Hajjaji, "Vehicle dynamic estimation with road bank angle consideration for rollover detection: Theoretical and experimental studies," *Vehicle Syst. Dyn.*, vol. 51, no. 12, pp. 1853–1871, Sep. 2013.
[28] X.-L. Tang, X. Hu, W. Yang, and H. Yu, "Novel torsional vibration modeling and assessment of a power-split hybrid electric vehicle equipped with a dual-mass flywheel," *IEEE Trans. Veh. Technol.*, vol. 67, no. 3, pp. 1990–2000, Mar. 2018. doi: 10.1109/TVT.2017.2769084.
[29] X. Tang, D. Zhang, T. Liu, A. Khajepour, H. Yu, and H. Wang, "Research on the energy control of a dual-motor hybrid vehicle during engine start-stop process," *Energy*, vol. 166, pp. 1181–1193, Jan. 2019.
[30] J. Na, Y. Xing, and R. Costa-Castelló, "Adaptive estimation of time-varying parameters with application to Roto-magnet plant," *IEEE Trans. Syst., Man, Cybern. Syst.*, to be published. doi: 10.1109/TSMC.2018.2882844.
[31] Y. Ma, C. Lu, H. Zhao, and M. Hao, "Nonlinear model predictive slip control based on vertical suspension system for an in-wheel-motored electric vehicle," in *Proc. 29th Chin. Control Decis. Conf. (CCDC)*, May 2017, pp. 4967–4972.
[32] Z. Zheng and M. Feroskhan, "Path following of a surface vessel with prescribed performance in the presence of input saturation and external disturbances," *IEEE/ASME Trans. Mechatronics*, vol. 22, no. 6, pp. 2564–2575, Dec. 2017.
[33] W. Sun, Z. Zhao, and H. Gao, "Saturated adaptive robust control for active suspension systems," *IEEE Trans. Ind. Electron.*, vol. 60, no. 9, pp. 3889–3896, Sep. 2013.
[34] G. Herrmann, M. C. Turner, and I. Postlethwaite, "Discrete-time and sampled-data anti-windup synthesis: Stability and performance," *Int. J. Syst. Sci.*, vol. 37, no. 2, pp. 91–113, Feb. 2006.
[35] Y. Huang, H. Wang, A. Khajepour, H. He, and J. Ji, "Model predictive control power management strategies for HEVs: A review," *J. Power Sources*, vol. 341, pp. 91–106, Feb. 2017.
[36] Y. Huang, A. Khajepour, M. Khazraee, and M. Bahrami, "A comparative study of the energy-saving controllers for automotive air-conditioning/refrigeration systems," *J. Dyn. Syst., Meas., Control*, vol. 139, no. 1, Oct. 2017, Art. no. 014504.
[37] J. J. Rath, M. Defoort, H. R. Karimi, and K. C. Veluvolu, "Output feedback active suspension control with higher order terminal sliding mode," *IEEE Trans. Ind. Electron.*, vol. 64, no. 2, pp. 1392–1403, Feb. 2017.
[38] C. Hu, H. Jing, R. Wang, F. Yan, and M. Chadli, "Robout H∞ output-feedback control for path following of autonomous ground vehicles," *Mech. Syst. Signal Process.*, vols. 70–71, pp. 414–427, Mar. 2016.
[39] Y. Qin, C. He, X. Shao, H. Du, C. Xiang, and M. Dong, "Vibration mitigation for in-wheel switched reluctance motor driven electric vehicle with dynamic vibration absorbing structures," *J. Sound Vib.*, vol. 419, pp. 249–267, Apr. 2018.
[40] Z. Wang, M. Dong, Y. Qin, Y. Du, F. Zhao, and L. Gu, "Suspension system state estimation using adaptive Kalman filtering based on road classification," *Vehicle Syst. Dyn.*, vol. 55, no. 3, pp. 371–398, Dec. 2016. doi: 10.1080/00423114.2016.1267374.
[41] Y. Qin *et al.*, "Speed independent road classification strategy based on vehicle response: Theory and experimental validation," *Mech. Syst. Signal Process.*, vol. 117, pp. 653–666, Feb. 2019. doi: 10.1016/j.ymssp.2018.07.035.
[42] M. Liu, F. Gu, and Y. Zhang, "Ride comfort optimization of in-wheel-motor electric vehicles with in-wheel vibration absorbers," *Energies*, vol. 10, p. 1647, Sep. 2017.
[43] Y. Qin, Z. Wang, C. Xiang, M. Dong, C. Hu, and R. Wang, "A novel global sensitivity analysis on the observation accuracy of the coupled vehicle model," *Vehicle Syst. Dyn.*, to be published. doi: 10.1080/00423114.2018.1517219.
[44] *Mechanical Vibration-Road Surface Profiles-Reporting of Measured Data*, document 8608-1995, ISO, 1995.
[45] Y. Qin, C. Xiang, Z. Wang, and M. Dong, "Road excitation classification for semi-active suspension system based on system response," *J. Vib. Control*, vol. 24, no. 13, pp. 2732–2748, Jul. 2018. doi: 10.1177/1077546317693432.
[46] C. Gorges, K. Öztürk, and R. Liebich, "Impact detection using a machine learning approach and experimental road roughness classification," *Mech. Syst. Signal Process.*, vol. 117, pp. 738–756, Feb. 2019. doi: 10.1016/j.ymssp.2018.07.043.
[47] J. Zhao, P. K. Wong, Z. Xie, X. Ma, and X. Hua, "Design and control of an automotive variable hydraulic damper using cuckoo search optimized PID method," *Int. J. Automot. Technol.*, vol. 20, no. 1, pp. 51–63, 2019. doi: 10.1007/s12239-018.
[48] Z. Wang, Y. Qin, L. Gu, and M. Dong, "Vehicle system state estimation based on adaptive unscented Kalman filtering combing with road classification," *IEEE Access*, vol. 5, pp. 27786–27799, 2017. doi: 10.1109/ACCESS.2017.2771204.
[49] M. Liu, J. Huang, and M. Cao, "Handling stability improvement for a four-axle hybrid electric ground vehicle driven by in-wheel motors," *IEEE Access*, vol. 6, pp. 2668–2682, 2018.
[50] Y. Qin, C. Wei, X. Tang, N. Zhang, M. Dong, and C. Hu, "A novel nonlinear road profile classification approach for controllable suspension system: Simulation and experimental validation," *Mech. Syst. Signal Process.*, to be published. doi: 10.1016/j.ymssp.2018.07.015.
[51] X. Liu and Q. Zhang, "New approaches to H∞ controller designs based on fuzzy observers for T-S fuzzy systems via LMI," *Automatica*, vol. 39, no. 9, pp. 1571–1582, Sep. 2003.

ZHENFENG WANG received the M.S. degree from Tsinghua University, Beijing, China, in 2012, and the Ph.D. degree in mechanical engineering from the Beijing Institute of Technology, China, in 2018. From 2017 to 2018, he was a Visiting Scholar with the University of Waterloo. He is working on the vehicle dynamics, state estimation, and modeling for vehicle and suspension systems. His research interests include vehicle dynamics and control, nonlinear state estimation, and controllable suspension systems.

YECHEN QIN received the B.E. degree and Ph.D. degree in mechanical engineering from the Beijing Institute of Technology, China, in 2010 and 2016, respectively, where he currently holds a Postdoctoral position. From 2013 to 2014, he was a Visiting Ph.D. Student with Texas A&M University, USA. From 2017 to 2018, he was a Visiting Scholar with the University of Waterloo. His research interests include controllable suspension systems, road estimation, and in-wheel motor vibration control.

CHUAN HU received the B.E. degree in vehicle engineering from Tsinghua University, Beijing, China, in 2010, the M.E. degree in vehicle operation engineering from the China Academy of Railway Sciences, Beijing, in 2013, and the Ph.D. degree in mechanical engineering from McMaster University, Hamilton, Canada, in 2017. He is currently a Postdoctoral Fellow with the Department of Mechanical Engineering, The University of Texas at Austin, Austin, USA. He has published more than 20 journal papers on leading journals in the automated vehicles areas. His research interests include vehicle system dynamics and control, motion control and estimation of autonomous vehicles, and robust and adaptive control. He is an Editorial Board Member of the international journal *Computer Simulation in Application* and *Journal of Advances in Vehicle Engineering*. He is also the Guest Editor of *Advances in Mechanical Engineering*.

MINGMING DONG received the degree in mechanical engineering from the Beijing Institute of Technology, China, in 2003, where he is currently the Director of the Noise and Vibration Laboratory. From 2017 to 2018, he was a Visiting Scholar with the University of Wollongong. His research interests include suspension system dynamics, in-wheel motor vibration control, modeling, and estimation, and modeling for lightweight vehicles suspension systems.

FEI LI received the B.E. and M.E. degrees in vehicle engineering from the Harbin Institute of Technology, Weihai, China, in 2004 and 2006, and the Ph.D. degree in vehicle engineering from Jilin University, Changchun, China, in 2010. He is currently an Assistant Chief Engineer with the Automotive Engineering Research Institute, China Automotive Technology and Research Center, Co., Ltd., Tianjin, China. His research interests include vehicle and tire dynamics and control, vehicle chassis recalibrating, and design and modeling for lightweight vehicles suspension systems.